**UNIVERSITY OF NAIROBI**

**SCHOOL OF ENGINEERING**

**DEPARTMENT OF CIVIL AND CONSTRUCTION ENGINEERING**

CRACK BEHAVIOUR UNDER VEHICULAR LOADING ALONG MBAGATHI ROAD IN

NAIROBI COUNTY

**SUBMITTED BY:**

**Njiru Joseph Mwaura     Reg No: F56/79945/2012**

A thesis submitted in partial fulfilment of the requirements for the Degree of Master of

Science in Civil Engineering in the department of Civil and Construction Engineering,

University of

Nairobi.

**MAY, 2016**

# DECLARATION

This thesis is my original work and has not been presented for a degree in any

other university

Signature:………………………………….

Date:                          31/05/2016

-----------------------------------------------------------

Njiru Joseph Mwaura

Reg. F56/79945/2012

## APPROVAL:

This thesis has been examined with my approval as university supervisor

i.    First Supervisor

Dr. S. Mumenya

Signature:………………………

Date:…………………………...

# ABSTRACT

Nairobi County has nearly 100% road network as bituminous roads and only 4km road network (Mbagathi Road) is concrete road. This road was a pilot project that was implemented by Kenyan Government between the years 2005 and 2007 at a total construction cost of over 400 million Kenya Shillings. The design was done based on South Africa design procedure on a 210 mm thick Plain Jointed Concrete Pavement (PJCP). Performance of Plain Jointed Concrete Pavement (PJCP) depends on aggregate interlock, which is the mechanism by which loads are transferred from one slab to the adjacent one. This study attempted to use the information on load transfer mechanics in order to quantify the effect of aggregate properties to crack size as well as the propagation of any cracks formed in service. Modern methods applied during the design of concrete pavement do not consider fracture mechanics into consideration. These make scheduling of repair and other maintenance works difficult.

This research was undertaken in two different ways namely experimental and computer simulation. The experimental approach entailed measuring widths and depths of cracks existing in Mbagathi road, and also involved setting up concrete beams in the laboratory and loading them to failure with predetermined loads and measuring sizes of resulting cracks. On the other hand, the computational approach was verified by experimental results entailed simulating crack widths and depths with recent devised fracture models.

Cracks were experimentally noticed to occur due to loading the pavement with vehicular loads bigger than safe load determined as 430.4kN. Cracks generated had crack width equivalent to the measured flexural deflection and for an ideal concrete pavement crack width and crack depth exhibited an exponential relationship. Experimental set-up yielded a deflection load curve that showed a quintic relationship, the maximum deflection recorded was 0.35mm.

It was found that vehicular loads induce stresses in concrete pavements which exceed permissible tensile stresses, hence a better understanding of the resultant cracks, as well as their propagation. Aggregate properties found to have an effect to crack width and depth were water to cement ratio, hardness and surface texture. This research will lead to an improvement of the design of concrete pavements in Kenyan environment.

# ACKNOWLEDGEMENT

## DEDICATION

This work is dedicated to my loving parents, Njiru Karigi and Ruth Runji, for all the sacrifices they made in my education. May the Almighty Father reward you according to His bountiful promise.

# TABLES OF CONTENTS

**LIST OF TABLES**

## LIST OF FIGURES

## LIST OF ACRONYMS AND ABBREVIATIONS

a          Space between inside clamps of the four point bending machine

A          Area

ADT        Average Daily Traffic

b          Width of the beam

BM        Beam

d          distance of the beam from the support to the clamps

CW        Crack width

D          Deflection

DJCP       Dowel Jointed Concrete Pavement

E          Young Modulus

Fc         Maximum force at point C .i.e. centre

G          Shear Modulus

h          Height of the crack in a beam

I          Moment of Inertia

$K_1$         Relationship factor for laboratory and theoretical deflections

kN         Kilo-Newton

L          Length

M          Moment

P          Load

PJCP       Plain Jointed Concrete Pavement

PUNDIT    Pulse Ultrasonic Non- Destructive Testing Machine

R          Radius of curvature

V          Shear force

w          Width of the crack in a beam

USA            United States of America

$\triangle$            Deflection

$\rho$            Curvature

$\theta$            Curvature angle (small angle)

N            Northing

E            Easting

El.            Elevation

**CHAPTER 1:  INTRODUCTION**

**1.1 Background Information**

Concrete material is inherently brittle hence susceptible to cracking when stresses exceed (tensile stress of 2.71N/mm$^2$ for concrete grade 35 [1]. Design of major highly loaded concrete pavements proposes a slab depth of 210mm [2]. Failure of concrete structures typically involves a stable growth of large cracking zones leading to fractures before the maximum load is achieved. Ordinary reinforced concrete design is not based on fracture mechanics. Even though it is known that prevention of brittle failures of concrete structures as a safety criterion, on concrete pavements will improve the economy. Concrete pavement was first constructed in Bellefontaine, Ohio; USA in 1893 [3]. The performance of several sections has and is still being monitored and the information has been used in upgrading design and construction methods. Since then Design of Rigid pavements have been done using firstly, analytical Solutions which are incorporated in numerical solutions. Later in 1965 Cheung and Zienkiewicz designed a pavement using finite element method where they analysed slabs on both liquid and solid type foundations [4]. Since then pavements of this nature have been designed in different countries [5]. Designers have not concentrated significantly on failure of these pavements [6]. This research focuses on a study where crack characteristics are investigated, which includes initiation, growth and eventual failure of pavement. This will add to knowledge regarding repair and maintenance in a timely manner. In this study, a computer method has been used to determine crack widths in pavements using available predictive models. This is useful information for design. It has been assumed that concrete slabs behaviour can be described as in theory of plates. This is supported by literature. For example, in 1986, Chudnovsky described "crack layer model" which considers the crack width as not being constant, as opposed to "crack band model" which considers it

constant [7]. The latter is the major predictive model for fracture in concrete pavements. [8].

The crack band model can be summarized as follows:

i.    The model characterizes material behaviour in the fracture process zone in a smeared manner through a strain- softening constitutive relation. In the smeared crack band, the crack opening 'w' is the product of average strain ($\varepsilon_{ave}$) and band width ($w_b$). i.e. $w = \varepsilon_{ave} * w_b$. This effect is quantitatively described as "softening damage" because the concrete surface suffers micro-cracking which leads to fracture.

ii.    The crack band model imposes a fixed width of front of the strain-softening zone. This fixed width represents a material property. Softening involves energy dissipation which can be quantified as a constant (fracture per unit length) which is the fracture energy of material.

In this research, vehicular loading is considered as the main contributor to cracking because the effects of temperature and humidity changes are insignificant. Because of their repetitive and adverse exposure nature, vehicular loading is closely related to fatigue of the loaded elements.

## 1.2 Problem Statement and Justification

In the past, design of concrete pavements has been undertaken using different design methods, which vary with different countries. The design does not take fracture mechanics in to consideration. This assumed that many concrete pavements would serve their design life even if fracture effects due to heavy vehicular loads were not incorporated. Introduction of fracture mechanics to concrete pavement design will enable predictions of initiation and propagation of existing or postulated cracks, hence, control of cracking through; repair and retro-filling would be better managed.

The results of this research will add value to the existing design specifications and philosophies, and in the long run, the comprehensive design approach will improve the durability of concrete road pavements. Hence, the repair and maintenance expenses would be minimized.

## 1.3 Main Objective

The main objective of this research is to assess and validate the fracture behaviour of existing cracks on a concrete pavement under vehicular loading over selected parts of Mbagathi road in Nairobi County.

## 1.4 Specific Objectives

- To review AASHO method (1986) and Crack band theory predictive models for crack growth.

- To use a chosen predictive model develop a simulation model for determination of theoretical crack widths using an appropriate predictive models.

- To determine the structural response on a typical concrete pavement due to different categories of vehicular loads.

- To validate the developed simulation model through comparison of theoretically, generated cracks widths and experimentally determined crack widths. .

## 1.5 Limitations

Many models for crack initiation and development which are utilised in design of concrete pavements are hypothesized and statistical in nature. This is because information required to refine the design models is still on-going.

**1.6 Hypothesis**

Major cracking in concrete pavements is attributed to fatigue caused by repetitive vehicular loads and the effects of variations in temperature and humidity are insignificant.

**CHAPTER 2:  LITERATURE REVIEW**

**2.1 Back ground information**

The principle of design of concrete pavements is flexure, similar to convectional beam design, therefore; bending strength of the slab is relied on to carry loads. In addition, the design is based on the presumption of continuous and uniform support, hence cannot be expected to perform as simply supported structures. For effective slabs on grade, performance depends on load transfer across cracks and joints. This is particularly critical on roads with heavy trucks and buses traffic. In general, cracks can be categorised as either hairline or large cracks. Hairline and narrow cracks are effective in utilization of interlocked concrete aggregates which can effectively transfer loads. However, wide cracks and widely spaced joints may open up under heavy loads cannot transfer loads across and must take higher edge loads. These higher edge loads can cause further cracking and deterioration at the joint or crack edges [7].

There are four types of concrete pavements namely:-

- Jointed plain concrete pavements

- Jointed reinforced concrete pavements

- Continuous reinforced concrete pavements

- Pre-stressed concrete pavements

A plain concrete pavement has no reinforcing steel and utilizes joints to control cracking. Joints may either be parallel to traffic (longitudinal joints) or perpendicular to traffic (transverse joints), warping and construction joints. Typical failure modes of jointed concrete pavement without an effective load- transfer mechanism include faulting, pumping, and corner breaks. These features of a plain concrete pavement are illustrated in Figure 2.1.

The key features of the pavement are: 20-25 cm stabilized cement base, which can be substituted with 21 cm recycled concrete MA 32 [1]. 5 cm thick asphalt layer uniformily laid over the base layer. 25 cm thick plain concrete pavement with 8 mm wide transverse joints at a spacing not exceeding 6m; longitudinal joints , dowelled bars grade 20/500 [1] and tie bars grade 14/700 [1].

Specifications of the pavement shown in figure 2.1 is as per European Union- Brite Euram III and journal on jointed reinforced concrete pavement [1, 29].
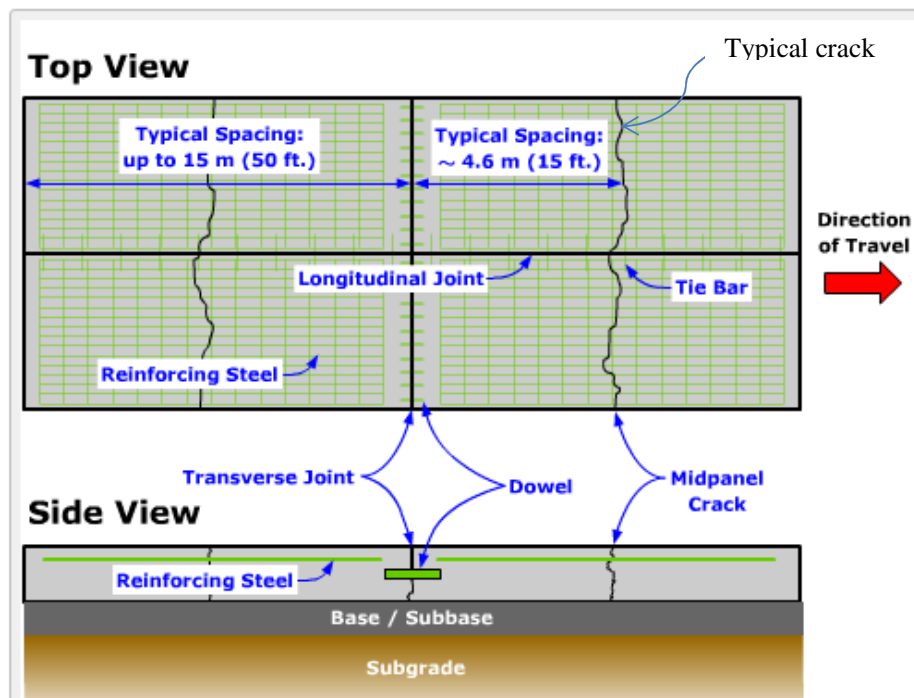


Figure 2.1: Typical cross-section of a concrete pavement showing key features.

## 2.2 Concrete quality

The long term structural integrity of a concrete pavement depends on:

i.   The selection of suitable materials.

ii.  Mix proportions for the concrete to be used.

iii. Workmanship and construction standards.

Selection of suitable materials used in concrete gradation has direct relationship with cracking. The coarse aggregate type   influences the amount of temperature expansion or contraction of concrete. Concrete that is more temperature sensitive has an increased potential for uncontrolled cracking. Limestone, granite and basalt have lower coefficients of thermal expansion than quartz, sandstones or siliceous gravels. These differences should be considered in design with a shorter spacing between contraction joints applied to concrete that is more temperature sensitive. The time of cracking may also be earlier for more temperature sensitive concrete. Field tests show that cracks form at the saw cut sooner and more frequently with concrete made from river gravel than concrete made with crushed limestone. ( [23-24]. Sand gradation also attributes to concrete quality, fine sand has high bulk volume due to higher volume of water used. For a good concrete mix sand of fineness modulus ranging between 2.3 to 3.1 is recommended, and not 45% of material should be retained in any sieve during sieve analysis. The strength of concrete is directly influenced by the quantity of cement and the water cement ratio. Increasing the quantity of cement and lowering the water cement ratio generally helps produce a denser and more durable mixture with higher early strength, but it may also contribute to a higher potential for uncontrolled cracking.

Workmanship in terms of jointing techniques, mixing of concrete and curing processes are among key influences to the resultant concrete quality [25].

## 2.3 Traffic Load

During its lifetime, a pavement is repetitively loaded by passing vehicles. The load of a single vehicle is converted to axles and wheel loads. Until now, vehicle loads in concrete pavement is modelled as static load and each type of joint provides a different ability to transfer load across slabs. This ability is termed as load transfer efficiency (or effectiveness). Load transfer

is important to pavement longevity. Most performance problems with concrete pavement are a result of poorly performing joints. Distress, such as faulting, pumping and corner breaks occur in-part from joints with poor load transfer efficiency. All of these problems worsen when joints deflect greatly under loads [3].

Load transfer between slabs may be provided by aggregate interlock, which is the mechanical locking which forms between the fractured surfaces along the crack below the joint saw cut [8].

Dowel bars provide a mechanical connection between slabs without restricting horizontal joint movement. They also keep slabs in horizontal and vertical alignment. When loaded by heavy vehicles, dowel bars lower joint deflection and stress in the concrete slab and reduce the potential for joint problems by increasing load transfer efficiency [3].

The use of dowel bars (smooth round bars) in transverse contraction joints primarily depends upon the roadway or street classification and can be determined by slab thickness [8]. Doweled contraction joints are not usually used in light to heavy residential or secondary urban pavements, but they are used in industrial roads, major streets, highways and airports that will carry heavy vehicles for long periods [3].

When dowels are not used, joints depend solely upon aggregate interlock for load transfer. Aggregate interlock is the mechanical locking which forms between the fractured surfaces along the crack below the joint saw cut. Reliance on aggregate interlock without dowels is acceptable on low-volume and secondary road systems where truck traffic is low and slabs are less than 200mm thick. Ordinarily, transverse joints with dowel bars provide better load transfer than those relying strictly on aggregate interlock [3].

Table 2.1 shows axle and wheel load spectrum as documented in durability design of concrete manual [2]

Table 2.1: Axle and Wheel load spectrum

| Wheel load (KN) | Axle load (KN) | Axle load Spectrum (%) Number of passes (%) | | |
|---|---|---|---|---|
| | | Light (Max weight 3.5 tonnes) | Average (Max weight 15 tonnes) | Heavy (Min weight 16 tonnes) |
| 10 | 0-20 | 7.6 | 5.4 | 4 |
| 20 | 20-40 | 25 | 22 | 15 |
| 30 | 40-60 | 30 | 29 | 26 |
| 40 | 60-80 | 18 | 20 | 27 |
| 50 | 80-100 | 11 | 12 | 14 |
| 60 | 100-120 | 6.1 | 7.7 | 8.4 |
| 70 | 120-140 | 1.8 | 3 | 4.4 |
| 80 | 140-160 | 0.41 | 0.75 | 1 |
| 90 | 160-180 | 0.07 | 0.1 | 0.12 |
| > 90 = 100 | > 160 = 180 | 0.02 | 0.05 | 0.08 |

The table shows that whereas, wheel load may be shown as a fixed value; axle load varies between two extreme values of a minima and maxima. Axle load spectrum which is given as a percentage is obtained using the following formula;

$$\frac{\text{Number of passes vehicles of that classification in a certain axle range}}{\text{Total Number of passes vehicles in that classification made}} \qquad \text{Equation 2.0}$$

For example, for a 10 KN wheel load the axle load spectrum for light spectrum was determined as number of passes made by vehicles of that weight for one hundred passes

counted, and so on for medium and heavy spectrum. The value given in table 2.1 can be

illustrated more clearly graphically as shown in figure 2.2.
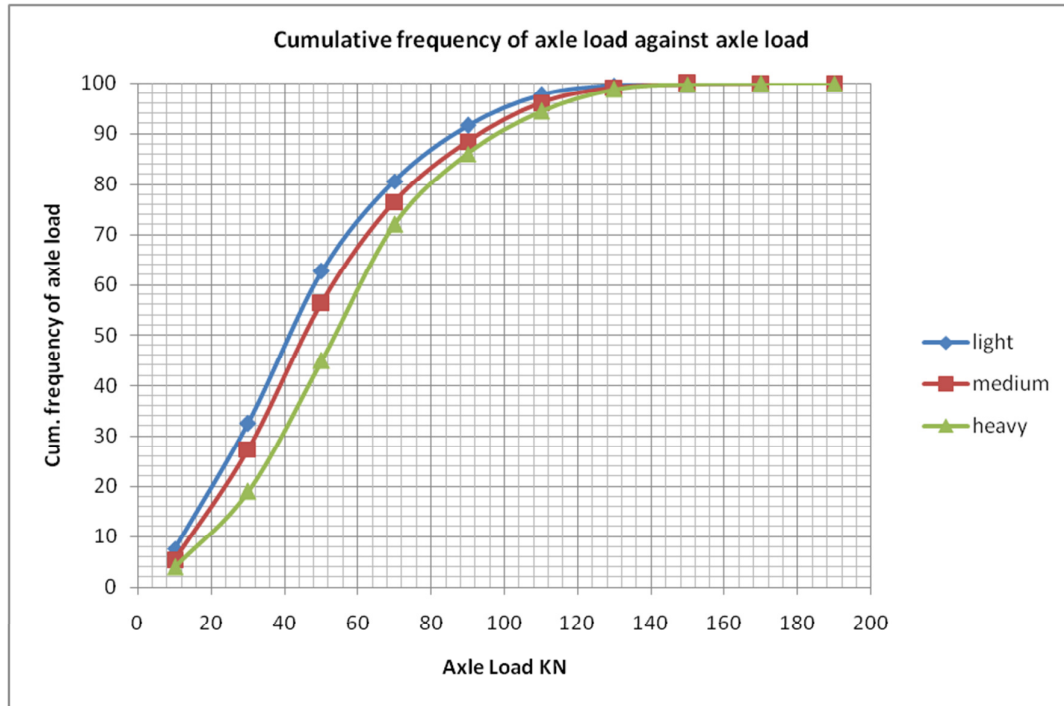


Fig 2.2: Cumulative frequency of axle load against axle load [2]

A spectrum is a condition or a specific property within a data range called continuum.

"Spectrum" characterizes the traffic on a pavement according to this characterization. Load

of a single vehicle is converted into to axle and wheel loads. For example, a vehicle has an

axle load classes of a bandwidth of 20kN where wheel load is 50% of the axle load i.e. half of

the upper limit of the axle load range. Heavy vehicles in the load spectrum enable

determination of stresses and stiffness on the pavement.

After getting the numbers of traffic in different wheel loads brackets, the numbers are

converted to percentages; for example number of light vehicles with an axle load in a certain

range divided with total number of light vehicles counted i.e.

$$\frac{Number\ of\ vehicles\ counted\ in\ range\ 0-20\ KN}{Total\ number\ of\ vehicles} = \frac{7.6}{100} * 100 = 7.6$$

and cumulative frequency determined for light, medium and heavy traffic as shown earlier in table 2.1. Light traffic represents vehicles with a weight lower than 3.5 tonnes, medium traffic vehicles have a weight range between 3.5 to 18 tonnes and heavy traffic vehicles have a weight above 18 tonnes. These values are used to plot the cumulative frequency curve as shown in figure 2.2.

**2.4 Behaviour of concrete pavements**

The function of a concrete road pavement is to support traffic loading and still maintain its rigidity and withstand deterioration effects over its design life. To achieve this, the pavement must enable the stresses in the subgrade caused by traffic loads to be maintained at a level that the subgrade can sustain without the development of cumulative permanent deformation, and without the development of elastic strains of a magnitude that would cause deterioration within the pavement.

When, under the action of wheel vehicular traffic, a concrete pavement slab is loaded to the point of rapture, the concrete fails in tension as a result of flexure rather than in compression. In a concrete pavement subject to flexure, the compressive and tensile stresses developed in the outer surfaces of the pavement are approximately equal. The tensile strength of concrete is much less than compressive strength [8]. When the load or bending moment increases to the point approaching rapture, the tensile stresses on the lower side of the pavement reaches the ultimate tensile strength before the compressive stress on the upper side of the pavement reaches the ultimate compressive strength.

In concrete pavement thickness design, the emphasis is centred on controlling horizontal tensile stresses at the lower surface of the concrete caused by this flexural action. The control of tensile strength is achieved by providing a sufficient thickness which in turn is largely dependent on the flexural strength of the concrete [9].

Fatigue in concrete is a progressive permanent internal structural damage when the concrete is subjected to repetitive stresses. Plain concrete when subjected to repetitive loads may exhibit excessive cracking and may eventually fail after sufficient number of load repetitions, even if the maximum load is less than the static strength of a similar specimen [10].

## 2.5 Steel area per slab in concrete pavement

Area of steel required for tie bars in the United States is calculated using sub grade drag theory, which is based on equilibrium of drag force of the concrete slab and maximum force that the tie bar can withstand without yielding [11]. Figure 2.1 in section 2.1 illustrates the relative positions of concrete slab and the tie bars. The sub grade drag in this system is expressed as given in equation 2.1.

$$A_S = \frac{b*h*W*f}{100S_s}$$ (Equation 2.1)

Where b is the width of pavement in mm, h is the depth of pavement in mm, W is the concrete unit weight (e.g. 2400kg/cm$^2$), f is the coefficient of friction ( i.e. 1.5), $S_s$ is allowable working stress in steel (e.g. 1750 kg/cm$^2$) and $A_s$ is the area of steel required to tie bars in mm$^2$.

## 2.6 Theory behind cracks formation, growth and control

Cracks occur in nearly all types of roads due to mechanical and environmental loadings. Cracking causes water penetration, weakening foundation of pavement structure and contributing to increased roughness. Engineering structures are designed to withstand the loads they are expected to be subject to while in service. Material imperfections at time of usage of the material are unavoidable; this leads to cracks formation on concrete surfaces. Due to continuous loading of the structure, the crack propagates and enlarges in the direction of critical stresses formation [12].

Crack initiation is related to stress, while crack growth is related to energy dissipation and high stresses surrounding the crack tip. Development of cracks can be quantified if both stress at which fracture starts ($\sigma$) and typical fracture energy to grow the crack by a unit area (G) is known. Many composite materials commonly used for pavement construction are quasi-brittle and are subjected to considerable size effects in fracture. Size effect is phenomenon where the strength of a structural system depends on its size [13]. Crack formation can be described using models; the main one being cohesive crack approach. This is implemented in Finite element method a modern method that finds many applications in engineering designs. Cohesive crack modelling was first introduced by Hillerborg [28]. In the model, a crack is induced when the stress in the material reaches its tensile strength. After the crack has formed, there exists stresses which still continue to be transferred across the crack through the mechanism of aggregate interlock, but the amount of stress transferred decreases with increase in crack width.

Formation of cracks in concrete is undesirable because it largely contributes to wear and deterioration of the whole structure. Cracking and its subsequent propagation can be controlled by appropriate design methods that consider crack reduction designs, materials selection and proportioning and construction practices. When a concrete pavement is being constructed, timing of joints as they are sawn and their depth is relevant [14].

## 2.7 Failure criteria

Above the elastic limits solid bodies respond to loading by undergoing large plastic deformations and for brittle materials fracture occurs soon after elastic limit is exceeded. Fatigue cracking is caused by load repetition that grows edge stress as found at mid slab where there are maximum moments. Other forms of failure in concrete elements include faulting (vertical displacement of abutting slabs at transverse joints creating a step in the

pavement), spalling (breakdown of crack edges) and joint deterioration (loss of original surface texture) [15].

## 2.8 Crack Propagation in Plates.

Griffith is regarded as the father of Fracture Mechanics; He observed experimentally that small imperfections have a much less damaging effect on the material properties than the large imperfections [16]. Griffith suggested an energy balance approach based not only on the potential energy of the external loads and on the stored elastic strain energy, but also on another energy term: the surface energy [16]. Formations of cracks results in induced strain energy which Griffith suggested a relationship given in equation 2.2.

$$U_{cracked} - U_{uncracked} = -\frac{2\pi*a^2*\sigma^2}{E} + \frac{\pi*a^2*\sigma^2}{E} + 4a\gamma \qquad \text{(Equation 2.2)}$$

Where a; is the crack length, and $\gamma$ is the unit weight of material, E is the young modulus for the material and $\sigma$ the stress in N/mm$^2$.

There are three types of cracking modes, namely Modes I, II, and III. Where Mode I is the tearing of a crack from tensile stresses, Mode II is the sliding of a crack due to in plane shear stresses and Mode III is the tearing of a crack due to out-of plane shearing [16].



Mode I                Mode II                Mode III
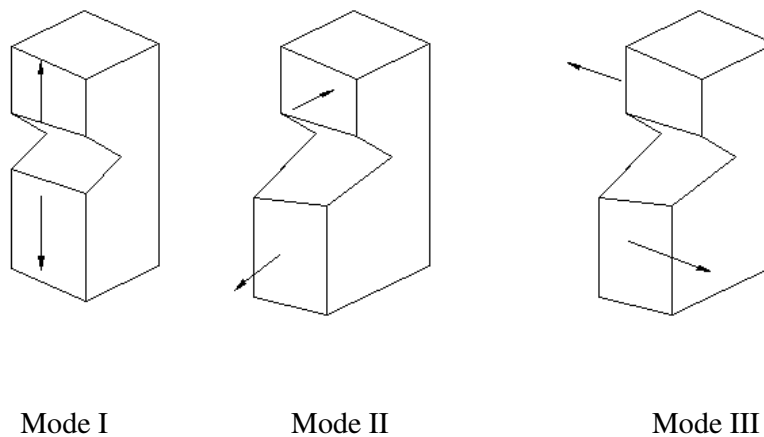
Fig 2.3: Modes of cracking

**2.9 Fracture Mechanisms**

Linear elastic fracture mechanism assumes all fracture process happens at the crack tip and the entire volume of the body remains elastic. The stress field which is made up of perturbation of trajectories of maximum principal stress, at the crack tip is singular. This means that stress components are the same regardless of loading and shape of body, with all the non-zero stress components approaching infinity as the radial distance "r" from crack tip tends to zero. The three stress components for the three cracking modes are related to stress intensity factors according to equation 2.3.

$$\sigma_{ij}{}^I = K_I f_{ij}{}^I \theta (2\pi r)^{-1/2} \ , \ \ \sigma_{ij}{}^{II} = K_{II} f_{ij}{}^{II} \theta (2\pi r)^{-1/2} \ , \sigma_{ij}{}^{III} = K_{III} f_{ij}{}^{III} \theta (2\pi r)^{-1/2}$$

(Equation 2.3)

Where subscripts I, II, III refers to the modes of cracking, and $\theta$ is planar angle and $K_I$, $K_{II}$, $K_{III}$ are stress intensity factors and $f_{ij}{}^I$ , $f_{ij}{}^{II}$ , $and$ $f_{ij}{}^{III}$ are tensile strength of concrete for cracking modes I, II, III respectively. [16].

**2.10 Non- Linear fracture models with softening zones for non-ductile materials**

This is where fracture zone is large and occupies nearly the entire non-linear zone [11]. The fracture process zone is the zone where material undergoes strain-softening i.e. stress normal to the crack plane decreases with increase in strain. Non-linear fracture is taken to occur within softening zone [11].

**2.11 Softening stress- strain relations**

The concrete cracks are never straight, but tortuous implying fracture zone can be described using stress- strain relations with strain softening. This approach is applicable in computer programming. There is no separation of nodes of two adjacent elements. Fracture process zone would therefore, be described as a zone in which material undergoes strain softening. Structurally, softening strains are modelled using stress displacement law; since it enables

internal cracking is well analysed [17]. Fracture is handled by adjustment of incremental stiffness of finite elements.

**2.12 Two dimension fracture matrix from crack band theory.**

The crack band theory states that, a heterogeneous aggregate material exhibits a gradual strain. Softening due to micro cracking and fracture is modelled as a blunt smeared crack band, which is justified by the random nature of the micro structure. Recent methods explain softening as being caused by fracturing strain $;\in^f$ which is superimposed on the elastic strain.

Hence, two dimensional matrix consists of these two types of strains. Related to this matrix is fracture energy which is the required energy for the formation and opening of micro-cracks per unit area of a surface plane. Compliance relationship relates strains and stresses as fracture energy opens the crack [4]. The relationship is given is given by equation 2.3. Compliance matrix is the matrix that relates the effect of cracks on the rate of creep.

$$\begin{Bmatrix} \epsilon_{11} \\ \epsilon_{22} \\ \gamma_{12} \end{Bmatrix} = \begin{Bmatrix} C_{1111} & C_{1122} & 0 \\ C_{2211} & C_{2222} & 0 \\ 0 & 0 & C_{1212}/\beta \end{Bmatrix} \begin{Bmatrix} \delta_{11} \\ \delta_{22} \\ \delta_{12} \end{Bmatrix} + \begin{Bmatrix} 0 \\ \epsilon^f \\ 0 \end{Bmatrix}$$ (Equation 2.3)

Where $\gamma_{12} = 2\epsilon_{12}$ , $c_{1111} = C_{2211} = C_{2222} = C_{2212}$ are elastic compliances and $\beta$ $is$ $a$ $constant$ $that$ $varies$ $from$ $0$ $to$ $1$

Fracture energy is obtained as $G_f = w_c \int_0^\infty \delta_{22}\, d\epsilon^f$ (Equation 2.4)

where $d\epsilon^f$ is the change in fracture strain. In many researches equations 2.3 and 2.4 are utilized. Cracking mode 1 and formulation of compliance matrices for partially or fully cracked concrete are the key procedures for computation of strains induced by principal stresses and extensions of cracks as they grow in evaluating sizes of cracks.

Though research to modern fracture mechanics is being done, atomic simulation method is not well researched on. In this latter method, inter atomic bonds are ruptured to allow crack

propagation and the method utilises using continuum solution for a cracked body under uniform tension, to calculate stresses and displacements.

## 2.13 Cohesive Zone Model.

The cohesive zone model provides a computationally efficient way to simulate damage occurring in a process zone located ahead of a crack tip. This approach involves non-linear constitutive laws described by the displacement jump and traction along the interfaces. It provides a phenomenological model to simulate fracture behaviour such as crack nucleation, initiation and propagation. Cohesive zone is the region between the material crack tip and the cohesive zone tip where complicated fracture behaviours, including inelasticity occur. The cohesive surfaces are joined together by a cohesive traction, which depends upon the displacement jump across crack faces. As the displacement jump increases due to an increase in external force or compliance in a structure, the traction first increases, then reaches a maximum, and finally decays monolithically to zero. The major cohesive parameters include material strength, critical displacement and cohesive fracture energy.

Cohesive model formulation can be described as shown below:

cohesive energy is obtained as   $G_f = w_c \int_0^\infty t \, d\delta$ 　　　　　(Equation 2.5)

Where t is the traction and $\delta$ is the normal displacement.

Fracture process zone is given by $\frac{\pi}{8} * \frac{E}{1-\vartheta^2} * \frac{G_c}{\sigma_{ave}^2}$ 　　(Equation 2.6)

Where $G_c$ is the cohesive energy, $\sigma$ is measure of material strength in the average sense, E is the young modulus and  $\vartheta$ is the Poisson ration for material [18].

## 2.14 Numerical Modelling.

The load spectrum tabulates and plots vehicular loads in a frequency curve as illustrated earlier on Fig 2.2 in section 2.3. Vehicular loads frequencies, cumulative frequencies, mean

and standard deviations are calculated, sorting out of critical loads for deflections and crack parameters calculations is done. Plates deform and crack after experiencing large deformations. Euler- Bernoulli beam theory is used in calculation of deflections at various locations of concrete slabs. Explicit methods for solving deflections are used in numerical modelling of concrete structures. Numerical integration method, utilizes the solution of the linear dynamic equilibrium equation written in the following form:

$$M\ddot{u} + C\dot{u} + Ku = F \qquad\qquad \text{(Equation 2.7)}$$

Where M is the mass matrix, C is damping matrix, K is stiffness matrix and $\ddot{u}, \dot{u} \text{ and } u$ are acceleration, velocity and displacement [22].

In this study, computational modelling utilized the following equations, which have been described in the next chapter; Equation 4.8, 4.9, 4.10, 4.11.

# CHAPTER 3: METHODOLOGY

## 3.1 Introduction

The methodology was based on the following:

i.    Assessment of structural strength of the pavement.

ii.   Analysis of wheel loads under different loading criteria and crack analysis on S-Math Studio platform. The platform was supported using the relationships given by equation 2.0 which were borrowed from the literature.

iii.  Analysis of crack widths on a typical concrete road crack.

iv.   Analysis of crack widths on laboratory cast beams.

## 3.2 Pavement condition survey

Pavement condition survey involves visual inspection to identify pavement distress features as cracks, potholes and deterioration. Washington State Department of Transport Damage model recommend a theoretical approach that determines percentage cracking index using pavement age and some controlled constants. i.e. C, p and m which represent initial state of pavement, degree of performance and slope coefficient respectively.

## 3.3 Wheel load effect on concrete pavement

The wheel load affects the pavement in many different ways. The research concentrated on effect of wheel load due to velocity, braking and turning effects. The position of wheel load on slab was also evaluated.

## 3.4 Analysis of Crack widths

The research analysed the formation of a crack on concrete pavement due to fatigue from repeated loading of heavy trucks. Once the cracks form the study concentrated on how cracks propagate and enlarge and eventually making the pavement unusable.

### 3.5 S-math studio

S-math studio was used in this research for analysis of cracks in concrete pavements due to heavy wheel loads

### 3.6 Expected output from the research

The expected results from the thesis research will include:-

- S-math studio analysis output and formulations from effect of wheel load due to breaking, velocity or turning.

- Crack widths for a typical concrete pavement (Mbagathi road).

- Crack widths for laboratory cast beams.

Crack widths were measured experimentally using the crack width gauge shown in Fig. 3.1. The machine accuracy was confirmed as 0.1mm.



Fig 3.1 Crack width Gauge used to measure cracks width

Crack depth was measured experimentally using the PUNDIT machine as shown below in Fig. 3.2. The machine was confirmed to have an accuracy of 0.1 microseconds for a selected path length of 400mm [19-21].
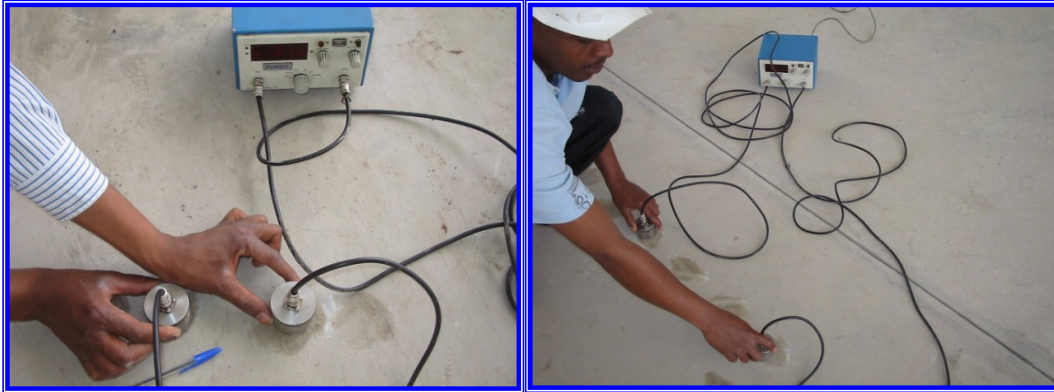
Fig 3.2 Ultrasonic Pulse Testing Machine used to measure cracks depth

# CHAPTER 4:  RESULTS, ANALYSIS AND DISCUSSION

## 4.1 Pavement Condition Survey

### 4.1.1 Visual Condition of Surface

Majority of pavement sections had not deteriorated, with majority of cracks and deterioration found at concrete slab joints. The slabs overall surface looked intact with minimum loss of surface texture.




Fig 4.1: Joint spalling at chainage 2450m
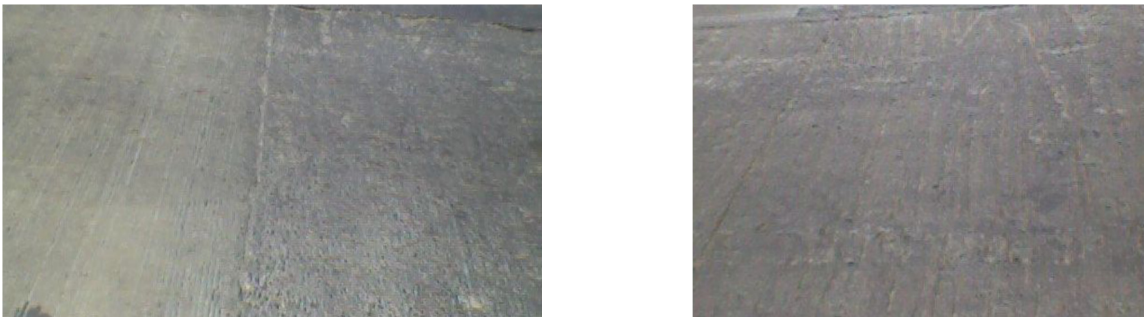



Fig 4.2: Road surface texture

### 4.1.2 Theoretical Pavement Condition Rating

The pavement condition index, which is the numeric representation of the pavement condition in the field, should have the same trends with time as field observations. For most pavements and

locations, the pavement condition tends to deteriorate at an ever increasing rate with time. The basic WSDOT PMS damage model was developed to represent this trend quite well. [25]

$$PCR = C - mA^P \hspace{3cm} \text{(Equation 4.1)}$$

where

PCR = Pavement Condition Rating

A = Pavement Age (time since construction or resurfacing)

C = model constant for maximum rating (100)

m = slope coefficient and

P = "selected" constant that controls the degree of the performance curve
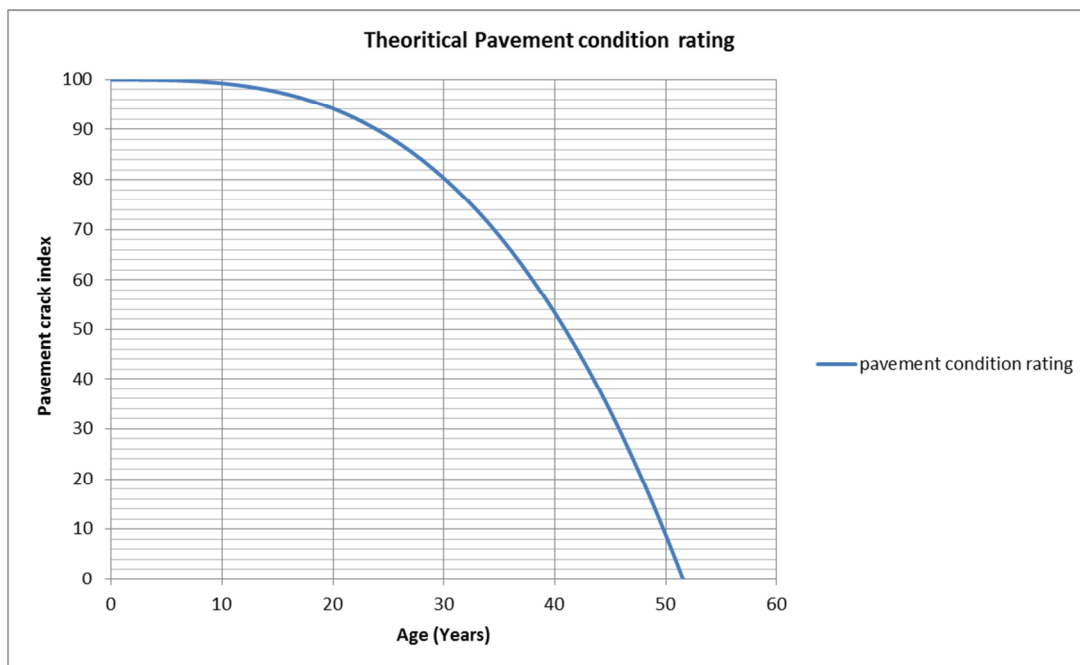


Fig 4.3: Theoretical pavement condition for Mbagathi road

**Discussion:**

Its nine (9) years since traffic was opened to Mbagathi road after commissioning in the year 2005. Theoretically, Mbagathi Road has a lifespan of 52 years after which a major re-carpeting can be done.

### 4.1.3 Pavement Cracking Index

It was calculated statistically. After walking through the pavement three sampling points were chosen after every 1.9 km. The points chosen were basically a stretch of 10m where major cracking was noticed. The locality of the points was as follows:-

Table 4.1: GPS Co-ordinates for sampling points 1, 2, 3 along Mbagathi road

| Sampling Point No. | Chainage | GPS Cordinates (UTM) |
|---|---|---|
| 1 | 1+900 | N 256136, E 9854573, El. 1673 |
| 2 | 3+800 | N 256500, E 9854641, El. 1673 |
| 3 | 5+700 | N 256866, E 9854779, El. 1667 |

The proposed pavement cracking index is based on the same approach that

WSDOT has used for the last 40 years and is shown as equation 1 earlier. It is assumed that

WSDOT will select its own term for this crack-based index.

RPCI = 100 - Σ Deducts                    (Equation 4.2)

The PCC pavement cracking distress was separated into three basic

categories of crack severity:

- Percentage of panels with 1 crack per panel

- Percentage of panels with 2 to 3 cracks per panel

- Percentage of panels with 4 or more cracks per panel

WSDOT has modified the way in which it classifies PCC pavement

cracking and is now categorizing PCC pavement cracking distress severity as follows:

- Number of panels (or %) with a single longitudinal crack (LC)

- Number of panels (or %) with a single transverse crack (TC)

- Number of panels (or %) with multiple cracks (MC)

Pavement distress deduct values have been developed for these last three

categories of cracking distress. The proposed RPCI is produced by summing the three

deduct values for a given section and subtracting the total value from 100. Because there

was no attempt to truncate the values as they approached 100, it will be possible to have negative

values under extreme conditions.

The resulting RPCI is:

$$RPCI = 100 - (LCDV + TCDV + MCDV) \qquad \text{(Equation 4.3)}$$

Where;

LCDV = Longitudinal Cracking Deduct Value

TCDV = Transverse Cracking Deduct Value

MCDV = Multiple Cracks Deduct Value

The recommended deduct values for PCC pavement cracking can be determined

from the following equations:

For Longitudinal Cracked Slabs use:

$$LCDV = 1.223(PLC)^{1.0437} \qquad \text{(Equation 4.4)}$$

Where;

LCDV = Longitudinal Cracking Deduct Value

PLC = Percentage of panels with longitudinal cracks

For Transversely Cracked Slabs use:

$$TCDV = 1.5038(PLC)^{1.0886} \qquad \text{(Equation 4.5)}$$

Where;

TCDV = Transverse Cracking Deduct Value

PTC = Percentage of panels with transverse cracks and for Multiple Cracked Slabs use:

$$MCDV = 2.2361(PMC)^{1.3495} \qquad \text{(Equation 4.6)}$$

Where;

MCDV = Multiple Cracking Deduct Value

PMC = Percentage of panels with multiple cracks

Table 4.2: Theoretical pavement cracking index for Mbagathi road

| | Rigid Pavement Cracking Index (RPCI) | | Panels checked in Mbagathi road |
|---|---|---|---|
| | For a span of 10m sampled | | 40 |
| | Longitudinal cracks | Transverse cracks | Multiple cracked slabs |
| No. of panel with said crack | 2 | 2 | 5 |
| Percentage (%) | 5 | 5 | 12.5 |
| | **LCDV** | **TCDV** | **MCDV** |
| | 6.56 | 8.67 | 67.57 |
| **RPCI** | **17.20** | as a percentage | |
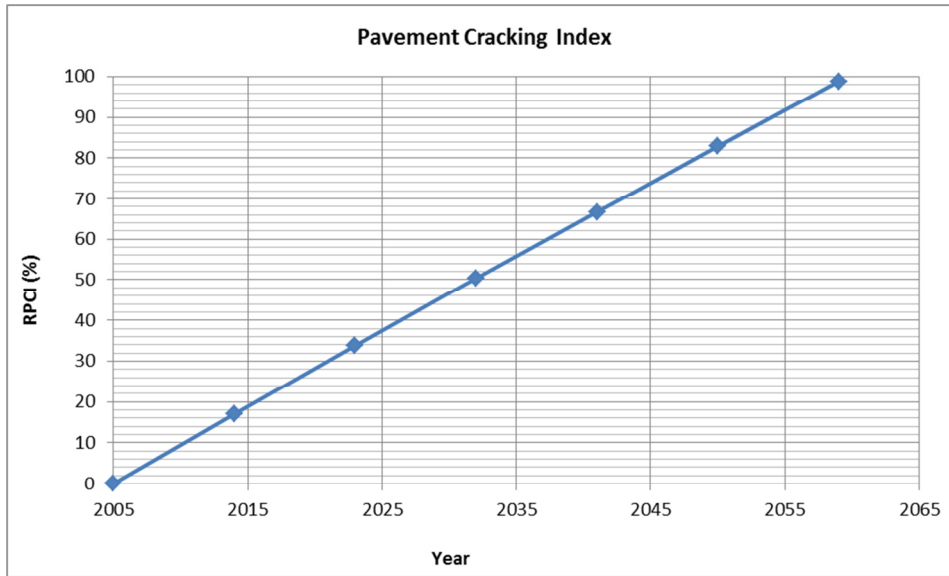
Fig 4.4: Theoretical pavement cracking index for Mbagathi road

**Discussion.**

The pavement crack index for Mbagathi Road has been estimated as 17.2% from 2005 to 2014 [25]. Considering cracks developing at the same rate, in the next 46 years the road will have fully cracked. Practically the design life for Mbagathi road can be taken as 55 years with the present traffic growth, after including the current age of 9 years. The graph above was based on real data from the time when condition survey was done in the year 2014 and when the pavement was opened to traffic in the year 2005. The other data for the years between 2015 to 2065 was based on extrapolation assuming a uniform gradient line.

The general equation relating the Pavement crack index with time is

$RPCI = 0.0013*t^2 + 1.9*t$; where t gives time from year of construction to the year of consideration

## 4.2 Road side traffic counts

Traffic counts were done at a location near the Mbagathi mosque. The traffic survey was conducted between 5th February, 2014 to 12th February, 2015 and 2nd March, 2015 to 9th March, 2015. This was the dry season of the year, and the environmental effect to the pavement was considered minimal. It was also considered at this time traffic flow was normal with less hindrances and vehicles would easily attain design speed all through the pavement. During this time of the year vehicular loading was the most critical source of internal stresses on the pavement therefore, ignoring environmental factors.

### 4.2.1 Recorded traffic counts

Table 4.3: Results of daily traffic counts

| Vehicle type | Mon | Tue | Wed | Thu | Fri | Sat | Sun | Totals | ADT |
|---|---|---|---|---|---|---|---|---|---|
| Bus | 885 | 893 | 865 | 578 | 981 | 359 | 206 | **4767** | 681 |
| MGV | 673 | 670 | 880 | 554 | 858 | 348 | 267 | **4250** | 607 |
| HGV | 169 | 203 | 196 | 155 | 234 | 94 | 34 | **1085** | 155 |
| A-HGV | 82 | 75 | 125 | 94 | 180 | 34 | 37 | **628** | 90 |
| Totals | **1809** | **1842** | **2066** | **1380** | **2254** | **835** | **544** | **10730** | **1533** |

### 4.2.2 Vehicle Equivalence Factor

The average vehicle equivalence factors have been derived from the maximum legal limits for vehicular loadings. The legal limits for equivalence factors are shown in table 4.3. The vehicle classes considered were:

   i.    Buses (B); passenger vehicles with more than 18 passengers;

ii. Medium Goods Vehicles (MGV); with 2 axles and un-laden weight above 1.5 tons;

iii. Heavy Goods Vehicles (HGV); vehicles having three or four rigid axles; and,

iv. Articulated Heavy Goods Vehicles (AHGV); vehicles with 3 or more articulated axles.

Table 4.4: Legal limits of vehicle equivalence factors in Kenya.

| Vehicle type | Maximum E.F based on legal limit |
|---|---:|
| Bus | 3.4 |
| MGV | 3.0 |
| HGV | 3.4 |
| A-HGV | 6.8 |

### 4.2.3 Design daily Equivalent Standard Axles

The design daily equivalent standard axles (DESA) were calculated by summing up product of average vehicle equivalence factors (VEF) and the average daily traffic (ADT) for both directions for each vehicle type. DESA for the most heavily loaded road section (at the mosque) was adopted for design. The Design daily Equivalent Standard Axles are shown in Table 4.4. Assuming that slow traffic lanes will carry 80% of commercial vehicles, the design traffic loading is 4,220 daily equivalent standards axles.

Table 4.5: Design daily Equivalent Standard Axles

| Vehicle type | V.E.F | Design ADT | DESA |
|---|---|---|---|
| Bus | 3.4 | 681 | 2315.4 |
| MGV | 3.0 | 607 | 1821 |
| HGV | 3.4 | 155 | 527 |
| A-HGV | 6.8 | 90 | 612 |
| **Totals** | | 1533 | 5275.4 |

## 4.3 Analysis using S- Math Studio

S-math studio is a mathematical solver with inbuilt functions inform of plugins developed in 2005 and runs in Microsoft Windows and Linux operating systems. It has a paper-like interface divided into two regions i.e. math region and text region. The developer (Andrey Ivashov) a Russian engineer made it possible for users to customise the solver according to need. The user can develop a plugin and apply it at the same time uploading open source plugins. This property gives it advantage over other available solvers such as Excel and Math-Cad. The computation interface allows the users to develop mathematical codes with any programming language. S-math studio was therefore used to develop a graphical user interface where crack width and depths were solved on various predictive models. Models where programed and their results displayed in the below attachments.

Model analysis of Crack width and spacings in Concrete Pavement
Model analysis will involve solutions to crack width, spacings and steel stress at crack using
AASHTO Method- 1986
INPUT

$ft := N$    psi    written as    $ft' := 441000$    | $\frac{n}{m2}$ |    load is a vertical load

$\alpha s := 0.00000645$

$\alpha c := 0.0000034$

$\theta := 0.75$

$\sigma w := 230$    $N = \frac{ft'}{6894.75729}$

$P := 0.58$

$Z := 0.0004$

$DTD := 60$

PROCESSES

  Crack Spacing Solutions    OUTPUT

$X := \frac{\left(1.32 \cdot \left(1 + \frac{ft}{1000}\right)^{6.7} \cdot \left(1 + \frac{\alpha s}{2 \cdot \alpha c}\right)^{1.15} \cdot (1+\theta)^{2.19}\right)}{\left(1 + \frac{\sigma w}{1000}\right)^{5.2} \cdot (1+P)^{4.6} \cdot (1+1000 \cdot Z)^{1.79}}$

$X = 0.3338$  inch

$x := X \cdot 25.4 = 8.4787$    mm

  Crack Width

$\Delta X := \frac{\left(0.00932 \cdot \left(1 + \frac{ft}{1000}\right)^{6.53} \cdot (1+\theta)^{2.20}\right)}{\left(1 + \frac{\sigma w}{1000}\right)^{0.491} \cdot (1+P)^{4.55}}$

$\Delta X = 0.0054$    inch

$\Delta x := \Delta X \cdot 25.4 = 0.137$    mm

  Steel stress

$47300 \cdot \left(1 + \frac{DTD}{100}\right)^{0.425} \cdot \left(1 + \frac{ft}{1000}\right)^{4.09}$

Ready    SlimDrivers    (100%)

File   Edit   View   Insert   Calculation   Tools   Pages   Help

Steel stress

$$\sigma s := \frac{47300 \cdot \left(1 + \frac{DTD}{100}\right)^{0.425} \cdot \left(1 + \frac{ft}{1000}\right)^{4.09}}{\left(1 + \frac{\sigma w}{1000}\right)^{3.14} \cdot (1 + 1000 \cdot Z)^{0.494} \cdot (1 + P)^{2.74}}$$

$\sigma s = 9359.0952 \quad psi$

$\sigma s1 := \sigma s \cdot 6.895 = 64530.9612 \quad kPa$

**Solutions for crack depth**

Moments    $L := 1 \quad m$    $H := 1 \quad mm$

$h := 0.21 \quad m$    +

$M := ft' \cdot \frac{L}{4}$  '''    $M = 1.085 \cdot 10^{5} \quad Nm$

$\sigma m := 6 \cdot \frac{M}{ft' \cdot h \cdot h} = 34.0136 \frac{n}{m2}$

$\sigma n := 1 - \sigma m = -33.0136$

$\frac{H \cdot x}{\Delta x} = 61.8774 \quad mm$    reported as crack depth

### 4.3.1 S-Math Studio

This platform was used to calculate crack width and depths for various traffic loading.

The theoretical maximum crack depth was calculated as 62mm based on the maximum traffic load received during survey. Crack width and crack depth were related by the following exponential relationship:

$$w = 3 * 10^{-18} e^{0.6206x} \dots \dots \dots \dots \dots \dots \dots \dots \dots \dots \dots \dots \dots \dots Equation\ 4.7$$

**crack width (mm) Vs crack depth (mm)**

$y = 3E\text{-}18e^{0.6206x}$
$R^2 = 1$

*(chart: Crack width (mm) on y-axis from 0 to 0.2; Crack depth (mm) on x-axis from 61.2 to 62.6)*

Legend:
— crack width Vs crack depth
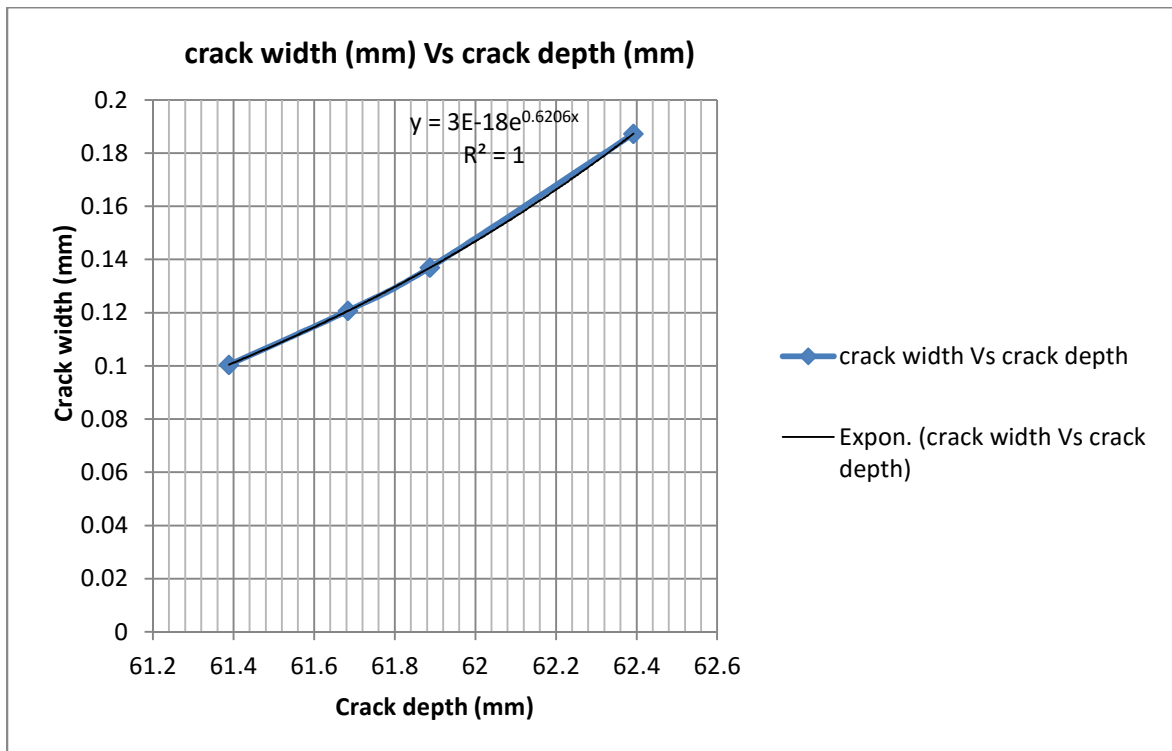— Expon. (crack width Vs crack depth)

Fig 4.5 Crack width against crack depth

## 4.4 Wheel load effect analysis

### 4.4.1 Cornering force

When a rolling pneumatic tyre is oriented in line with its direction of travel, the cornering

force is zero. When the tyre is subjected to a transverse force, an angle is created

between the direction of the tyre heading and the direction of travel. This angle is known

as the slip angle. For small angles of slip, the cornering force increases linearly with slip angle. For larger slip angles, the cornering force increases nonlinearly with slip angle at a reducing rate. The cornering force also increases non-linearly with vertical load at a reducing rate.

$$F=\mu mv^2/r \hspace{4cm} \text{Equation 4.8}$$

Increase in turn radius, reduces the slip angle reducing the scuffing forces hence less effect on cracking of a concrete pavement.

**4.4.2 Wheel load velocities**

High velocities increase scuffing forces hence more effect to cracking of concrete. Due to load not transferred and the vertical load increases (Eqn. 4.1)

**4.4.3 Wheel load effect on parking or stationary**

Stationary loads have the least effect to concrete pavement. In this research their contribution to cracking is negligible due to load not transferred to nearby concrete pavement slabs hence scuffing forces are zero, so no noticed concrete cracking.

**4.5 Concrete crack analysis**

The concrete crack analysis was done in accordance to AASHTO Guide for Design of Pavement Structures.

Crack spacing, crack width and steel stress at crack were evaluated as follows:

$$X=\frac{1.32\ (1+\frac{f_t}{1,000})^{6.70}*\left(1+\frac{\alpha_s}{2a_c}\right)^{1.15}*(1+\varnothing)^{2.19}}{(1+\frac{\sigma_w}{1,000})^{5.20}*(1+p)^{4.60}*(1+1,000Z)^{1.79}} \hspace{2cm} \text{Equation 4.9}$$

$$\Delta X = \frac{0.00932\ (1+\frac{ft}{1{,}000})^{6.53}*(1+\varnothing)^{2.20}}{(1+\frac{\sigma_w}{1{,}000})^{0.491}*(1+p)^{4.55}}$$

Equation 4.10

$$\sigma_S = \frac{47300\ (1+\frac{DT_D}{100})^{0.425}*(1+\frac{ft}{1{,}000})^{4.09}}{(1+\frac{\sigma_w}{1{,}000})^{3.14}*(1+p)^{2.74}+(1+1{,}000Z)^{0.494}}$$

Equation 4.11

Where $f_t$ is the concrete tensile strength (N/m$^2$), $\sigma_w$ is tensile stress due to wheel loads (N/m$^2$), $p$ is percentage of steel, $\varnothing$ is the diameter of steel, $Z$ is the concrete shrinkage coefficient, $\alpha_s$ is steel thermal coefficient (mm/mm/$^o$c) and $a_c$ is concrete thermal coeffient (mm/mm/$^o$c)

### 4.6 Experimental Crack depth determination

Crack depth for the Mbagathi road was determined at four different chainages using ultrasound equipment. These chainages were 0+212, 0+420, 1+600, 1+890 and 2+242. The ultrasound method measures crack depth using time of flight the wave uses to penetrate an identified crack. The crack depth is determined using the following expression

$$h = x\ \sqrt{\frac{4T_1{}^2 - T_2{}^2}{T_2{}^2 - T_1{}^2}}$$

Equation 4.12

Where $x$ is the distance between crack and transducer and $T_1$ and $T_2$ are the time-of-flight of the longitudinal wave with transducers at distances $x$, and $2x$ from the crack, respectively. The table below represents the experimental results for crack depth estimation on selected sections of Mbagathi road.

Table 4.6: Experimental results for crack depth and width

| Method assumes transducers equidistant | | | | | Measured Crack width (mm) | Chainage and GPS Coordinates |
|---|---|---|---|---|---|---|
| Crack no. | x (cm) | T1 | T2 | h (cm) | | |
| 1 | 15 | 4.8 | 6 | 8.673608 | 0.4 | 0+212 N 255524, E 9856193, El. 1722 |
| 2 | 15 | 5.8 | 7 | 9.033071 | 0.4 | 0+420 N 255466, E 9856001, El. 1720 |
| 3 | 15 | 8 | 9 | 11.67243 | 0.5 | 1+600 N 255876, E 9854909, El. 1691 |
| 4 | 15 | 12 | 13 | 12.10454 | 0.5 | 1+890 N 256025, E 9854660, El. 1676 |
| 5 | 15 | 8.2 | 9 | 14.94533 | 0.7 | 2+242 N 256352, E 9854584, El. 1660 |
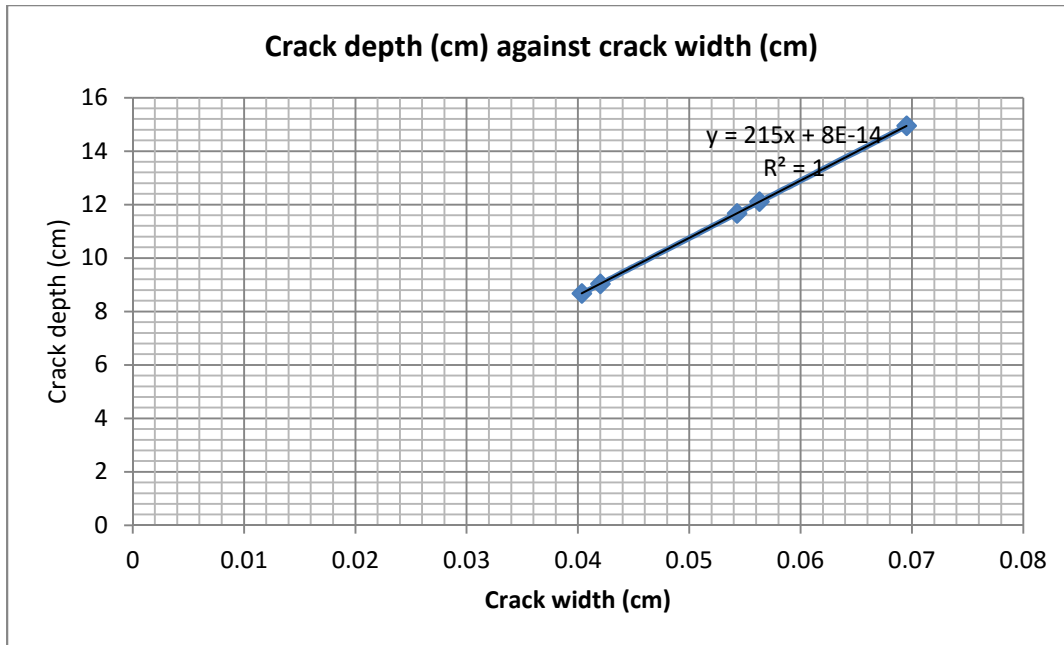
Fig 4.6 Experimental crack depth against crack width

**Discussion**

Out of the measured slabs, there was no slab that was fully cracked since there is no crack depth of up to 215mm which is the thickness of the slabs. However, as the crack depth increased, the crack width increased since as the crack forms there is more opening towards the bottom of the slab.

## 4.7 LABORATORY TESTS

### 4.7.1 Procedure

The method employed in the laboratory test was:

a) Performing sieve analysis for fine and coarse aggregate to be used in the preparation of beams.

b) Preparing mix design for concrete class 30 and a Young Modulus of $29000N/mm^2$.

c) Construction of a timber mould for preparation of beams dimension 200mm wide, 215mm deep and 1000mm long. Whose geometric properties are:-

Area (A) = 43000 mm$^2$

Moment of inertia (I) = 165,639,583.33mm$^4$

d) Casting of 10 no. beams for flexural tests and analysis using four- point bending approach.

**4.7.2 Beams Mould**

The figure below illustrates the mould used to cast the beams, which was typically made from timber and bolts (8mm wide) as

connections.
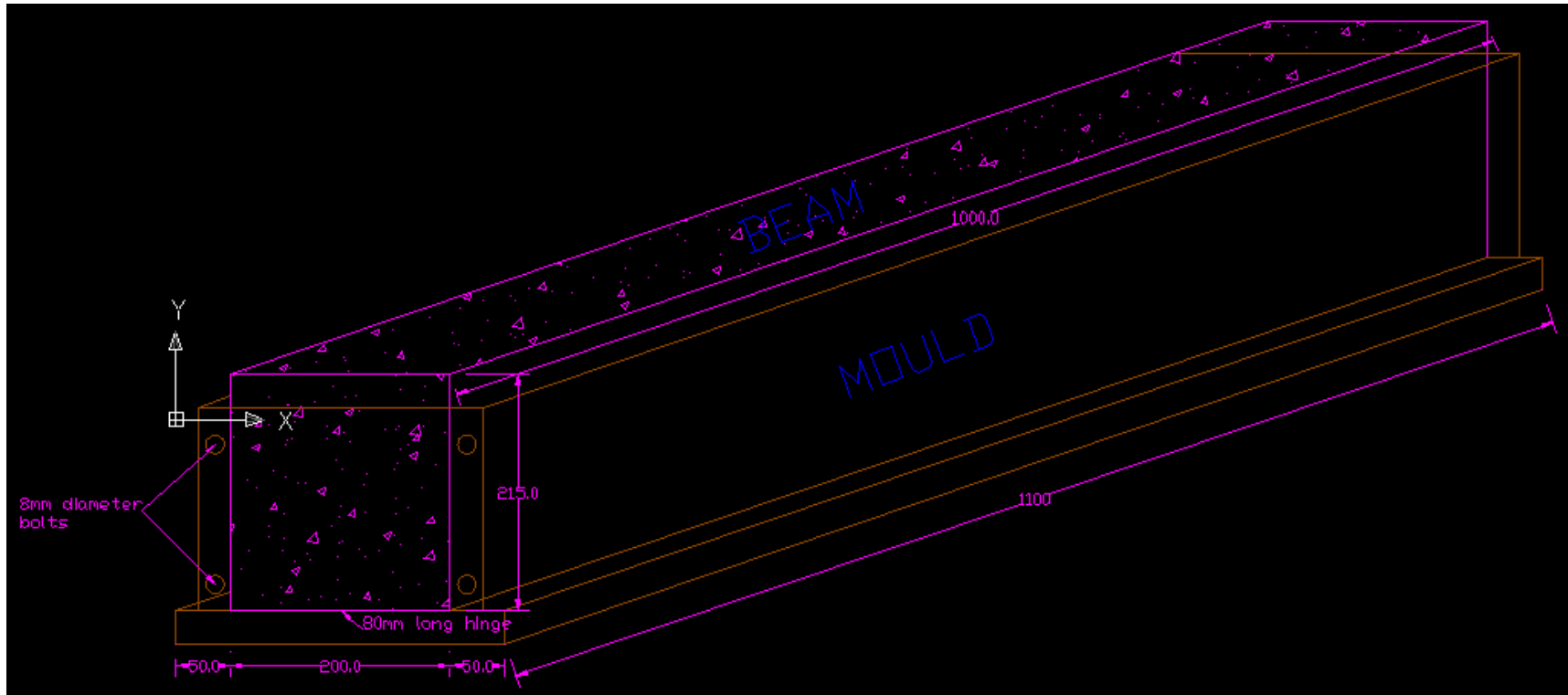


Fig 4.7: Design drawing for the mould

### 4.7.3 Sieve Analysis

The sieve analysis for both fine and coarse aggregate was done for sand and aggregates. The sieves were arranged from largest to smallest. Later the data was filled and analysed in the below sheets.

Table 4.7: Sieve analysis for coarse aggregate Sieve (mm)

| Two kilograms of coarse aggregate was used. | Mass retained (g) | Cumulative mass passing (g) | Cumulative percentage passing | Max (%) | Min (%) |
|---|---|---|---|---|---|
| 37.5 | 0 | 2000 | 100 | 100 | 100 |
| 28 | 100 | 1900 | 95 | 100 | 90 |
| 20 | 300 | 1600 | 80 | 95 | 65 |
| 10 | 500 | 1100 | 55 | 70 | 40 |
| 6.3 | 250 | 850 | 42.5 | 55 | 30 |
| 2 | 250 | 600 | 30 | 40 | 20 |
| 1 | 130 | 470 | 23.5 | 32 | 15 |
| 0.425 | 130 | 340 | 17 | 24 | 10 |
| 0.075 | 200 | 140 | 7 | 10 | 4 |
| less than 0.075 | 140 | 0 | 0 | 0 | 0 |

Yielding the below grading curve
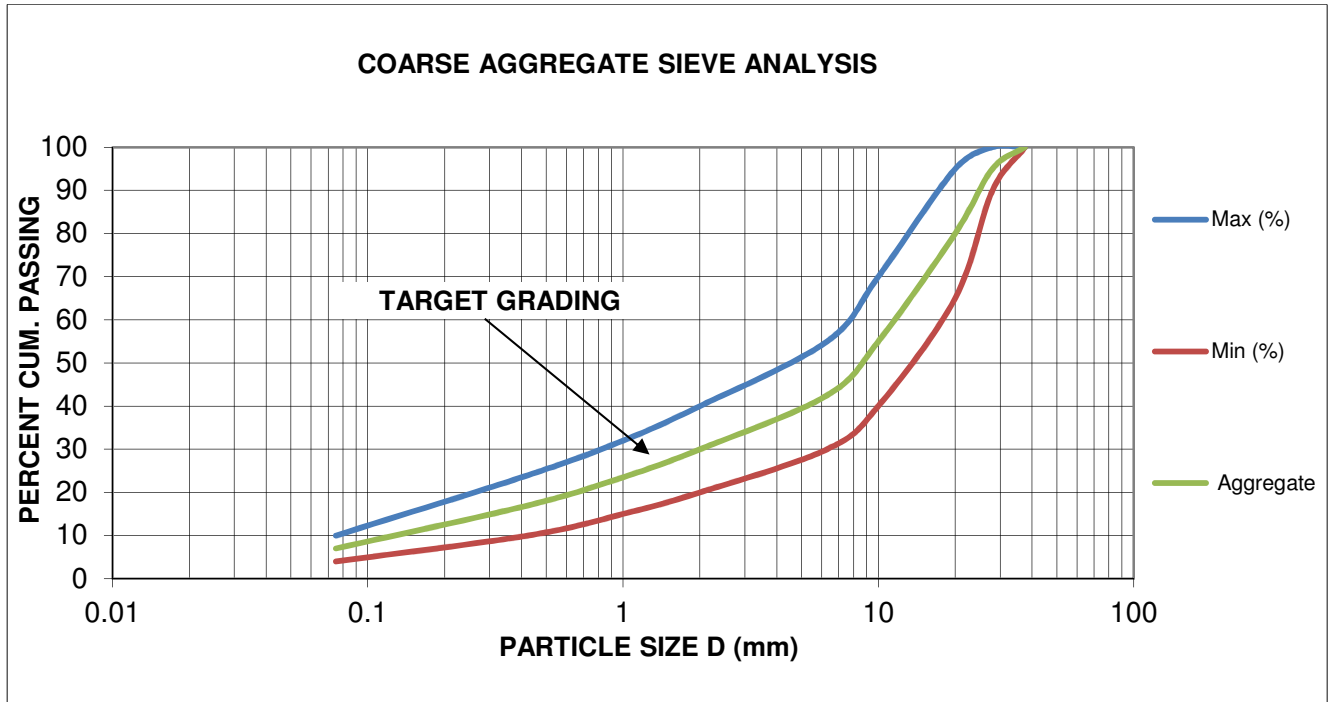


Fig 4.8: Grading curve for coarse aggregate

**Summary.**

The coarse aggregate had 28mm nominal maximum size. Fineness Modulus is the Cumulative Percentage Retained up to particle size 150μm= 357/100= 3.57. A higher value of fineness modulus indicates the aggregate is well graded.  Coarse aggregate is well graded since it falls in between maximum and minimum curve of the target curve. Fineness modulus is inversely proportional to surface area. Aggregate with higher fineness modulus require little cement paste and little water since the area is small.

### 4.7.4 Sieve analysis for the Fine aggregate

One kilogram of fine aggregate was used and the results are as shown in Table 4.8

Table 4.8:  Sieve analysis for fine aggregate

| Sieve (mm) | Mass retained (g) | Cumulative mass passing (g) | Cumulative percentage passing |
|---|---|---|---|
| 10 | 0 | 1000 | 100 |
| 4.75 | 52 | 948 | 94.8 |
| 2.36 | 30 | 918 | 91.8 |
| 1.18 | 86 | 832 | 83.2 |
| 600um | 258 | 574 | 57.4 |
| 300um | 328 | 246 | 24.6 |
| 150um | 207 | 39 | 3.90 |
| less than 150um | 39 | 0 | 0 |

Yielding the below grading curve



Fig 4.9: Grading curve for fine aggregate

**Summary.**

Fine aggregate has effective size of 0.19mm and a uniformity coefficient of 3.4.

$D_{10}$= 0.19mm
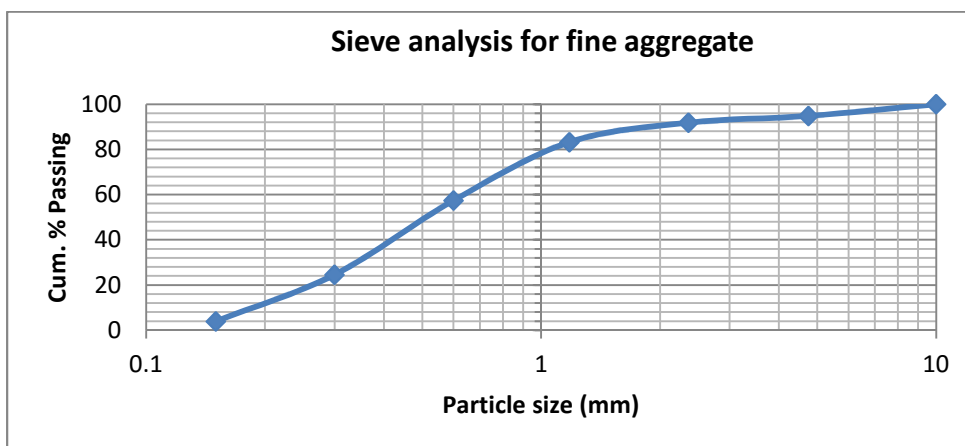
Uniformity Coefficient = $D_{60}/D_{10}$ =0.65/0.19 = 3.4

Fineness Modulus is the Cumulative Percentage Retained up to particle size 150µm= 344/100= 3.4. A higher value of fineness modulus indicates the aggregate is well graded. Fineness modulus is inversely proportional to surface area. Aggregate with higher fineness modulus require little cement paste and little water since the area is small.

### 4.7.5 Mix Design.

Done in accordance to IS 456:2000. The mix ratio for coarse aggregate, fine aggregate, cement and water was done. Concrete cubes were cast using different Mix rations.

Water cement ratio was selected between a range of 0.3 to 0.42 and three concrete cubes cast for each selection with the same mix proportion for cement, sand and coarse aggregate.

Crushing strength showed mix proportions of 1:2:3 for cement, sand, aggregate and 0.42 water/cement ratio respectively yielded a target mean strength of 30N/mm$^2$ and adopted to cast the beams.

Below are the results for the Mix Design.

a) Water Cement Ratio of 0.42

   Target mean strength:      30N/mm$^2$

Cement Type          : Ordinary Portland cement 32.5N (Bamburi) with a specific gravity of

3.15

Fine aggregate:          River sand with a specific gravity of 2.5

Coarse aggregate:          Crushed stone was rounded and relatively large size with a specific

gravity of 2.64

Mixing Proportion:  0.42: 1: 2: 3 for water, cement, fine and coarse aggregate respectively.

Slump                : 80mm. This shows there was a good workability on the utilised concrete.

Table 4.9: Cube strength for water cement ratio of 0.42

| Cube No. | | Crushing Strength (N/mm$^2$) | |
|---|---|---|---|
| | Mass (Kg.) | 7 days | 28dys |
| C-01 | 8.1 | 14 | 22 |
| C-02 | 8.0 | 15 | 24 |
| C-03 | 8.1 | 13 | 24 |
| **Average** | | **14** | **23.4** |
| **Standard deviation** | | **4** | |
| **Target Mean Strength** | | **23.4 + 4* 1.65** | **30 N/mm$^2$** |
| **Comment** | | **Mix Design acceptable and adopted** | |
| **Discussion** | | **This water cement ration was adequately checked thorough several trial mixes and the recorded strength was ascertained. The achieved strength was the actual pavement strength during the time of construction. This was** | |

| | | **according to field and daily reports at Ministry of Infrustructure offices; Nairobi.** |
|---|---|---|

b) Water Cement Ratio of 0.3

Target mean strength  :        30N/mm2

Cement Type  : Ordinary Portland cement 32.5N (Bamburi) with a specific gravity of 3.15

Fine aggregate:                River sand with a specific gravity of 2.5

Coarse aggregate:              Crushed stone with a specific gravity of 2.64

Mixing Proportion:  1: 2: 3 for cement, fine and coarse aggregate respectively

Table 4.10: Cube strength for water cement ratio of 0.3

| **Cube No.** | | **Crushing Strength (N/mm$^2$)** | |
|---|---|---|---|
| | **Mass (Kg.)** | **7 days** | **28dys** |
| C-04 | 7.8 | 19 | 30 |
| C-05 | 7.7 | 20 | 29 |
| C-06 | 7.8 | 20 | 30 |
| **Average** | | **20** | **30** |
| **Standard deviation** | | **4** | |
| **Target Mean Strength** | | **30 + 4* 1.65** | **37 N/mm$^2$** |
| **Comment** | | **Mix Design not acceptable** | |

c) Water Cement Ratio of 0.35

Target mean strength  :        30N/mm2

Cement Type  : Ordinary Portland cement 32.5N (Bamburi) with a specific gravity of 3.15

Fine aggregate:                     River sand with a specific gravity of 2.5

Coarse aggregate:                   Crushed stone with a specific gravity of 2.64

Mixing Proportion:  1: 2: 3 for cement, fine and coarse aggregate respectively

Table 4.11: Cube strength for water cement ratio of 0.35

| Cube No. | | Crushing Strength (N/mm$^2$) | |
|---|---|---|---|
| | Mass (Kg.) | 7 days | 28dys |
| C-04 | 7.9 | 17 | 26 |
| C-05 | 7.9 | 16 | 25 |
| C-06 | 7.8 | 17 | 25 |
| **Average** | | **16.7** | **25.3** |
| **Standard deviation** | | **4** | |
| **Target Mean Strength** | | **25.3 + 4* 1.65** | **32 N/mm$^2$** |
| **Comment** | | **Mix Design not acceptable** | |

## 4.7.6 Flexural Test

Four point bending test was considered for this research. Four point bending test has the maximum flexural stress spread over the section of the beam between loading points avoiding premature failure. Peak stresses are along an extended region, hence larger length of the specimen would be analyzed for defects. Whereas, three point test has stress concentrated at the center of the loading point where the stress is at peak.

Four point bending test presents the case of loading in the actual pavement, since the wheel load effect has a tendancy of spreading all-over the beam.

Four point bending test has flexural stress, strain, stiffness and deflection calculated as below:-

Flexural stress; $\quad\quad\quad\quad\sigma_f = \dfrac{3aP}{bh^2}$ $\quad\quad\quad\quad\quad\quad$ (Equation 4.7.6)

Flexural strain; $\quad\quad\quad\quad\varepsilon_f = \dfrac{12hP}{3L^2 - 4a^2}$ $\quad\quad\quad\quad$ (Equation 4.7.7)

Stiffness; $\quad\quad\quad\quad\quad S = \dfrac{\sigma_f}{\varepsilon_f}$ $\quad\quad\quad\quad\quad\quad\quad$ (Equation 4.7.8)

Deflection (Maximum); $= \Delta = \dfrac{d(4d^2 - 3L^2)\, P}{24EI}$ $\quad\quad\quad$ (Equation 4.7.9)

## 4.7.7 Flexural Results

The ten (10) cast beams were subjected to four point bending test, at an age of 7 and 28 days and the below results were produced after 28 days flexural test:

Five beams each for 7 days and 28 days respectively have a statistical viability since the results tabulated have an error reduced by 20% compared to only using one beam in each test.

Error reduction factor = 1/p $\quad\quad\quad\quad\quad\quad\quad\quad$ (Equation 4.7.10)

Where p represents the number of items i.e. 5, for this research five was used because it's the best choice between 1 to 5 where many researches numbers lies.

Beam No. 1

Table 4.12: Flexural strength test results for Beam No. 01

| Deflections | | | Cracks formed | | | |
|---|---|---|---|---|---|---|
| P (kN) | D (mm) | B-01 | Major | Minor | w (mm) | h(mm) |
| 0 | 0 | | 2 | <10 | 1 | 120 |
| 0.5 | 0.05 | | | | 0.5 | 89 |
| 1.5 | 0.1 | | | | | |
| 2.5 | 0.15 | | | | | |
| 3 | 0.2 | | | | | |
| 3.4 | 0.35 | | | | | |
| 3 | 0.5 | | | | | |
| 2.5 | 0.6 | | | | | |
| 2 | 0.7 | | | | | |

Beam No. 2

Table 4.13: Flexural strength test results for Beam No. 02

| Deflections | | Cracks formed | | | |
|---|---|---|---|---|---|
| P (kN) | D (mm) | Major | Minor | w (mm) | h(mm) |
| 0.0 | 0.0 | 2 | <10 | 0.8 | 114 |
| 0.5 | 0.0 | | | 0.5 | 85 |
| 1.4 | 0.1 | | | | |
| 2.3 | 0.1 | | | | |
| 2.8 | 0.2 | | | | |
| 3.1 | 0.3 | | | | |
| 2.8 | 0.5 | | | | |
| 2.3 | 0.6 | | | | |
| 1.8 | 0.6 | | | | |

Beam No. 3

Table 4.14: Flexural strength test results for Beam No. 03

| Deflections | | | Cracks formed | | | |
|---|---|---|---|---|---|---|
| P (kN) | D (mm) | B-01 | Major | Minor | w (mm) | h(mm) |
| 0.0 | 0.0 | B-03 | 2 | <10 | 0.9 | 130 |
| 0.5 | 0.0 | | | | 0.7 | 93 |
| 1.4 | 0.1 | | | | | |
| 2.3 | 0.1 | | | | | |
| 2.8 | 0.2 | | | | | |
| 3.2 | 0.3 | | | | | |
| 2.8 | 0.5 | | | | | |
| 2.3 | 0.6 | | | | | |
| 1.9 | 0.7 | | | | | |

Beam No. 4

Table 4.15: Flexural strength test results for Beam No. 04

| Deflections | | | Cracks formed | | | |
|---|---|---|---|---|---|---|
| P (kN) | D (mm) | B-01 | Major | Minor | w (mm) | h(mm) |
| 0.0 | 0.0 | B-04 | 2 | <10 | 1 | 122 |
| 0.5 | 0.0 | | | | 0.5 | 85 |
| 1.4 | 0.1 | | | | | |
| 2.4 | 0.1 | | | | | |

| 2.8 | 0.2 | | | | | |
|---|---|---|---|---|---|---|
| 3.2 | 0.3 | | | | | |
| 2.8 | 0.5 | | | | | |
| 2.4 | 0.6 | | | | | |
| 1.9 | 0.7 | | | | | |

Beam No. 5

Table 4.16: Flexural strength test results for Beam No. 05

| Deflections | | | Cracks formed | | | |
|---|---|---|---|---|---|---|
| P (kN) | D (mm) | | Major | Minor | w (mm) | h(mm) |
| 0.0 | 0.0 | B-05 | 2 | <10 | 1 | 118 |
| 0.5 | 0.0 | | | | 0.6 | 83 |
| 1.4 | 0.1 | | | | | |
| 2.4 | 0.1 | | | | | |
| 2.9 | 0.2 | | | | | |
| 3.3 | 0.3 | | | | | |
| 2.9 | 0.5 | | | | | |
| 2.4 | 0.6 | | | | | |
| 1.9 | 0.7 | | | | | |

## Load Deflection Curve

Load Deflection Curve was plotted for all the beams and yielded the following results:-



**Load deflection curve for four point bending test**

$$y = 2104.7x^6 - 4804.1x^5 + 4193.9x^4 - 1705.1x^3 + 285.22x^2 - 0.0468x - 0.006$$
$$R^2 = 0.9992$$

- Load deflection curve BM # 01
- Load deflection curve for BM # 02
- Load deflection curve BM #03
- Load deflection curve BM # 04
- Load deflection curve BM # 05
- Poly. (Load deflection curve BM # 01)
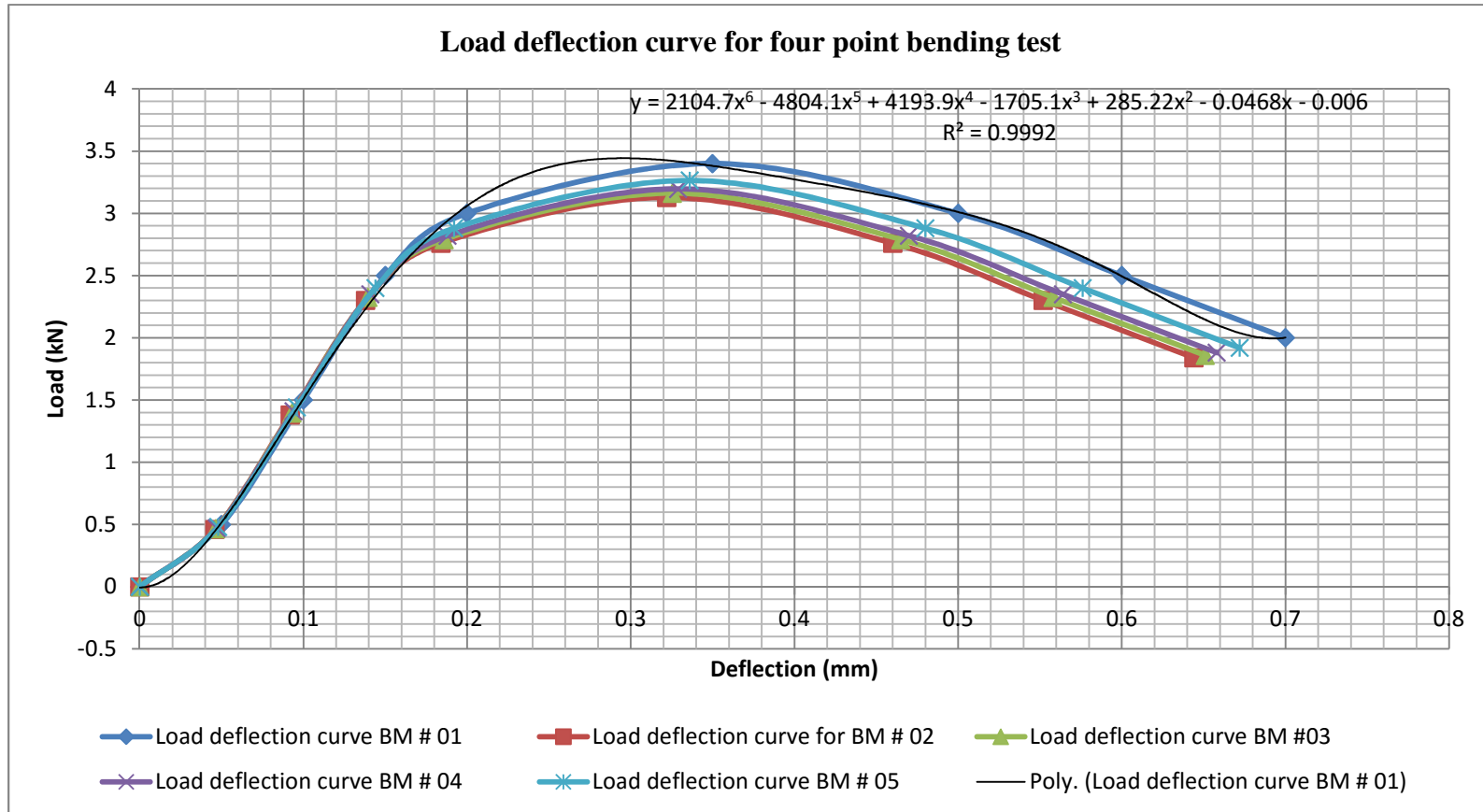
Fig 4.10: Load against mid-span deflection for the tested beams

**Discussion.**

The beams subjected to flexural test were prepared with dimensions of a design of a representative sample of the depth of the pavement i.e. depth of Mbagathi road slab. The length was based on one metre design criteria. These criteria allowed direct relationship of laboratory, experimental and field testing data. For all the beams tested, the resultant cracks were less than ten and only one to two cracks were visible without magnifying lenses and their results were tabulated.

Fracture energy to induce the maximum crack is calculated as the area under beam number 01 divided by fracture area, which was calculated as the area under load deflection curve as illustrated here below.

$\int_0^{0.7} 2104.7 * x^6 - 4804.1 * x^5 + 4193.9 * x^4 - 1705.1 * x^3 + 285.2 * x^2 - 0.0468x^1 -$ 0.006 = 1.779 kN-mm or 1.779 Nm

Fracture area is given by crack width * depth of the crack = 0.6mm * 83 mm = $4.98*10^{-5}$ m$^2$

Total fracture energy G$_F$ = $\frac{\text{Area under Load vs Deflection}}{\text{fracture area}}$ = $\frac{1.779}{0.0000498}$ = **35.72KJ**

In conclusion a maximum fracture energy of **35.72** KJoules is required to initiate cracking in 200mm by 215mm by 1000mm beams. Traffic loads generating more energy than 35.72 KJoules would cause fracture in the concrete pavement and traffic loading should be limited to a maximum load which yields 35.72 KJ.

Energy/ Work done = Force * Distance (depth of the crack i.e. 83mm)

Force = Energy/ Distance = 35.72/ 0.083 = 433.06 = **430.4 kN**

**Inference**

A maximum wheel load of 430.4kN is the maximum safe load on Mbagathi road pavement.

**4.7.8 Concrete Beams Cracking**

Beams were loaded to failure on four point bending machine. Initially deflection increases with increase in loading, after failure the load decreases as deflection slightly increases. Major cracks formed were longitudinal and transverse, where the transverse were the most critical cracks since they were easily noticed, wide and deep; while longitudinal cracks were very small and not easily noticed i.e. micro-cracks.

Generally, two transverse cracks were highly noticed on every beam tested; and these were cracks which were measured and their data presented as above.



Fig 4.11: Major transverse cracks across the beam

## 4.8 Derivation and application of Theories of Beams Deflections

Deformation of beams is majorly from deflection. The main methods used to analyse deflection in elastic structures are geometric methods which utilises the strain of an elastic structure to determine the deflection and the Energy methods which are based on the principle of conservation of energy. There are several theories which explain deflections of beams. They are as explained below.

### 4.8.1 Castigliano's Method

The theorem states that, when a body is elastically deflected by any combination of loads, the deflection at any point and in any direction is equal to the partial derivative of strain energy (computed with all loads acting).
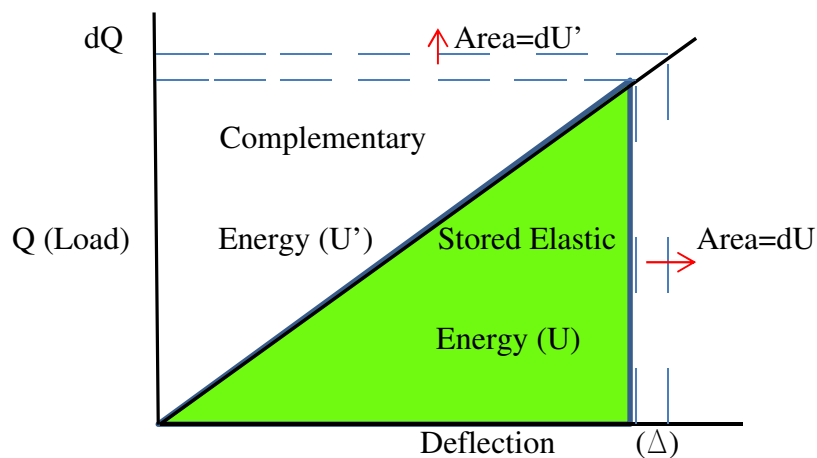


Fig. 4.12: Energy stored in a deflected beam

The following equations can be deduced;

$$U = U' = \Delta.\ Q/2$$

Small areas consideration, or incremental; $dU = dU' = \Delta.dQ$, .i.e. area of a rectangle.

Deflection; Δ= dU/dQ, hence castigliano theorem written as:

$\Delta \ = \ \partial U / \partial Q$; Elastic deflection for a beam centrally loaded, reflects the beams scenario as tested for flexural test in the research.

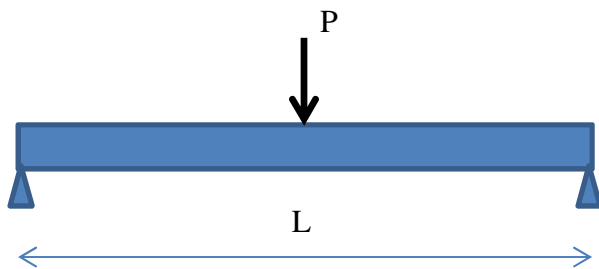The beam is analysed as below: considering bending and transverse shear
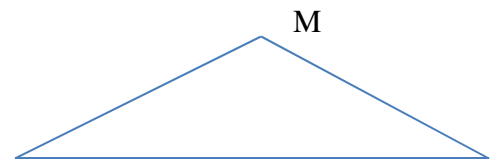


Fig. 4.13: A simply supported beam centrally loaded          Fig. 4.14: Moment diagram for

the beam

The resultant deflection is derived as below:

$$\Delta = \int_0^{L/2} \frac{M(\frac{\Delta M}{\Delta P})}{EI} dx + \frac{\Delta}{\Delta P} \quad = \quad 2* \int_0^{L/2} \frac{M^2}{2*EI} + \int_0^L \frac{3*V^2}{5*G*A}$$

Where M = $\frac{Px}{2}$ and V= P/2

$$\Delta = 2* \int_0^{L/2} \frac{P^2 x^2}{8EI} dx \ + \int_0^L \frac{3 (\frac{P}{2})^2}{5GA} dx$$

$$\Delta = \frac{P*L^3}{48EI} + \frac{3PL}{10GA} \qquad\qquad \text{(Equation 4.8.1)}$$

### 4.8.2 Conjugate- beam method

The method proposes construction of a beam with the same length as the real beam referred to as conjugate beam. The conjugate beam is loaded with the M/EI diagram, simulating the external load w. The shear and moments developed in the conjugate beam correspond to the slope and the displacement condition of the real beam. Deflection and slope for a beam centrally loaded is developed as follows.
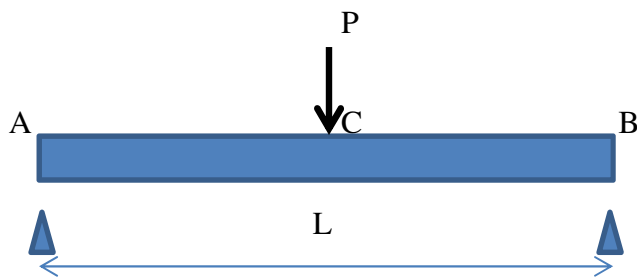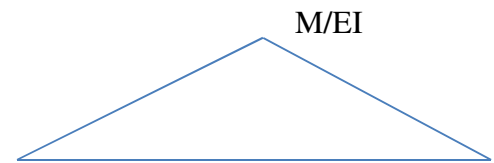
Fig. 4.15: A simply supported beam centrally loaded          Fig. 4.16: M/EI diagram for    the
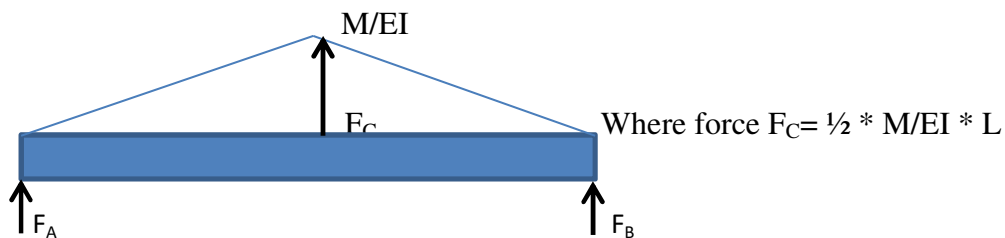
beam

Fig. 4.17: Conjugate beam loaded with M/EI

Where force $F_C$= ½ * M/EI * L
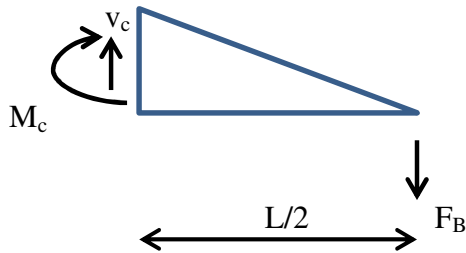
Summing moment at A and equating downward and upward forces.

$$\sum M_A = 0 = \frac{1}{2} * \frac{M}{EI} * L * \frac{L}{2} + F_B * L \qquad so \qquad F_B = -\frac{ML}{4EI}$$

$F_A$+ $F_B$= $F_C$; follows that $F_A = -\dfrac{ML}{4EI}$

Breaking the beam, and taking the moment at point C, then the deflection action at the point is developed;



$$\Sigma M_C = 0 = \frac{1}{2} * \frac{M}{EI} * \frac{L}{2} * \frac{L}{6} - F_B * \frac{L}{2} \qquad\qquad so \qquad F_B = -\frac{ML}{4EI}$$

$$M_C = \frac{ML^2}{24EI} - \frac{ML^2}{8EI} = \frac{ML^2}{24EI} \qquad \text{replacing } M=P*L/4 \qquad\qquad \text{(Equation 4.8.2)}$$

$$\Delta = \frac{P*L^3}{48EI} \qquad\qquad \text{(Equation 4.8.3)}$$

### 4.8.3 Double integral method

This method is also known as Macaulay's method. Developed from, strain and curvature of a beam .i.e. equations of elastic curve.

$$Strain = \frac{\Delta L}{L} \; and \; also \; to \; \frac{\sigma}{E}, \text{ stress } (\sigma) \; = \; \frac{Mc}{I}$$

$$\frac{c}{\rho} = \frac{Mc}{EI} \; ; \quad or \quad \frac{1}{\rho} = \frac{M}{EI} \qquad\qquad \text{(Equation 4.8.4)}$$

From calculus, curvature is given by; $\dfrac{1}{\rho} = \dfrac{\dfrac{d^2 y}{dx^2}}{[1+\left(\dfrac{dy}{dx}\right)^2]^{\frac{3}{2}}}$ for most beams the slope is small i.e. $\dfrac{dy}{dx}$

is small and its square is much smaller, Hence the denominator would be ignored.

$$\frac{1}{\rho} = \frac{d^2 y}{dx^2}$$

(Equation 4.8.5)

Equating equation 4.1.4 and 4.1.5, the double integral deflection equation for the beam is

developed.

$$EI\frac{d^2 y}{dx^2} = M(x)$$

(Equation 4.8.6)

Where y, is the deflection determined by double integrating the equation and applying the

boundary conditions.

$$y_{\text{A-B}} = \int_{X_A}^{X_B} \theta dx = \iint_{X_A}^{X_B} \frac{M}{EI} dx$$

(Equation 4.8.7)

Solving for simply supported beam loaded at centre by a point load; the resultant deflection is:

$$\Delta = \frac{P*L^3}{48EI}$$

(Equation 4.8.3)

**4.8.4 Dummy Load method**

The method is based on use of unit dummy (virtual) load applied on the structure in the direction

where the deformation is to be determined. The basis of the method starts from the moment

curvature equation.

$$d\Theta = \left[M(x) * \frac{1}{EI}\right]dx$$

In this theorem, the order of loading does not change the final value of deformation.

Work done by $F_1$ due to deflection at point 2, is equal to work done by $F_2$ due to deflection at point 1. Considering bending only, the real deformation is only $d\Theta$.

Therefore, dummy load theorem can be concluded as

$$1.0 * (v_p \text{ or } \Theta p) == \int m(x)\left[\left[M(x) * \frac{1}{EI}\right]dx \right] \qquad \text{(Equation 4.8.8)}$$

For a simply supported beam centrally loaded, a deformation at centre is calculated as follows.
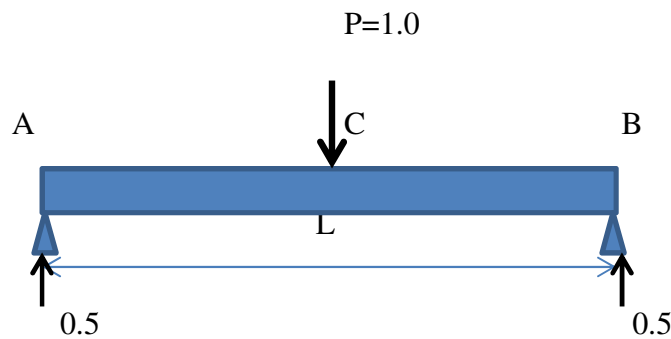


Moment equations for the virtual beam are; 0 <L/2; m(x) = 0.5x and for L/2 < x < 2, m(x) = 0.25L-0.5x;

The same equations for the real beam changes to 0 <L/2; m(x) = P/2*x and for L/2 < x < 2, m(x) = 0.25PL- 0.5P*x; applying the principle conservation of energy; External work done equals the internal work done.

$$1 * d_c = \int \frac{mM}{EI}dx = \int_0^{L/2} 0.5x * P/2 * x dx + \int_{L/2}^{L}(0.25L - 0.5x) * (0.25PL - 0.5Px)dx =$$

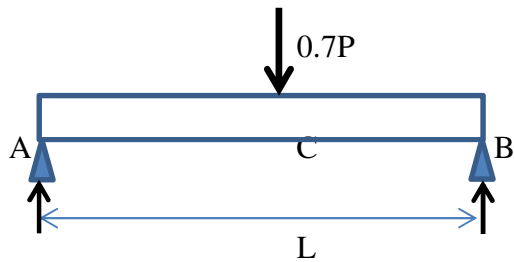$$\Delta = \frac{P * L^3}{48EI}$$

## 4.8.5 Superposition method

Slope and deflection of a beam due to several loads, is equal to the sum of those due to the individual loads. Procedure is facilitated by tables of solutions for common types of loadings and supports.
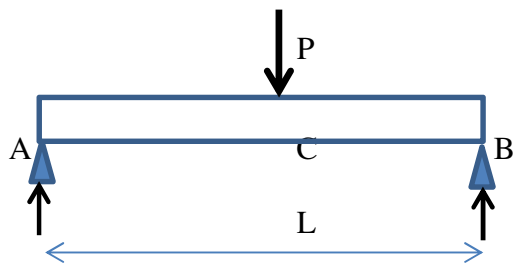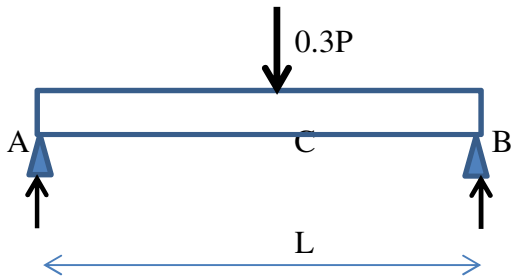


$$\Delta = \frac{P * L^3}{48EI}$$

=



$$\Delta_1 = \frac{0.7P * L^3}{48EI}$$

+

$$\Delta_2 = \frac{0.3P*L^3}{48EI}$$

$\Delta = \Delta_1 + \Delta_2$                                           (Equation 4.8.9)

## 4.8.6 Moment Area method

Commonly used method to compute slopes and deflections in beams and frames. The area of the bending moment diagrams is utilised for computing the slope and deflections at particular points along the axis of the structure.
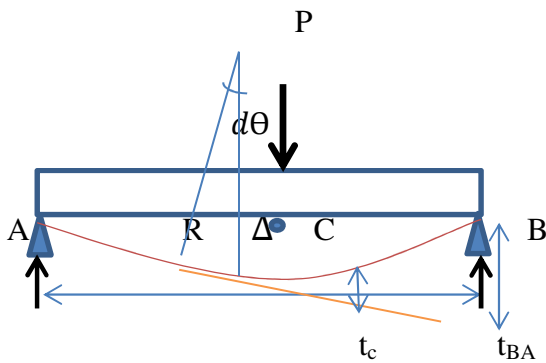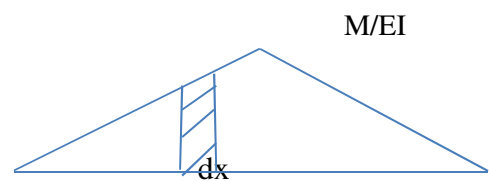


Fig. 4.18: M/EI diagram for    the beam



Fig. 4.19: M/EI diagram for    the beam

The derivation of deflection equation starts with bending equation.

$$\frac{M}{I} = \frac{E}{R}$$  (Equation 4.8.9)

$$dx = d\Theta * R$$  (Equation 4.8.10)

Substituting for R;  $\Delta\theta_{AB} = \int_A^B d\Theta = \int_A^B \frac{M}{EI} \, dx$ ; i.e. area of M/EI diagram

$\theta_A * L = t_{AB}$ where; $t_{AB} = \int_A^B \frac{Mx}{EI} \, dx$ ;

$$\theta_A = \frac{1}{L} * \left(\frac{1}{2} * \frac{PL}{4EI} * L * \frac{L}{2}\right) = \frac{PL^2}{16EI}$$  (Equation 4.8.11)

$$\theta_A - \theta_B = \left(\frac{1}{2} * \frac{PL}{4EI} * L\right) = \frac{PL^2}{8EI}$$  (Equation 4.8.12)

$$\theta_A * \frac{L}{2} = \Delta + t_{CA}$$

$$\frac{PL^2}{16EI} * \frac{L}{2} = \Delta + (\frac{1}{2} * \frac{PL}{4EI} * \frac{L}{2} * \frac{L}{6})$$

$$\Delta = \frac{P*L^3}{48EI}$$

## 4.9 Theoretical and Laboratory Comparison

### 4.9.1 Theoretical and Laboratory Testing

Theoretical determinations considered the beam at elastic conditions, while the laboratory methods yielded deflections at both elastic and plastic state of the beam. In this research, the comparison done was for elastic state of the beam. Deflection load curves were draw and the resultant equations were compared as illustrated below.

### 4.9.2 Theoretical and Laboratory Deflections and comparative graph

The two approaches had the following data for loads and resultant deflections.

Table 4.17: Theoretical and laboratory deflections at various loads

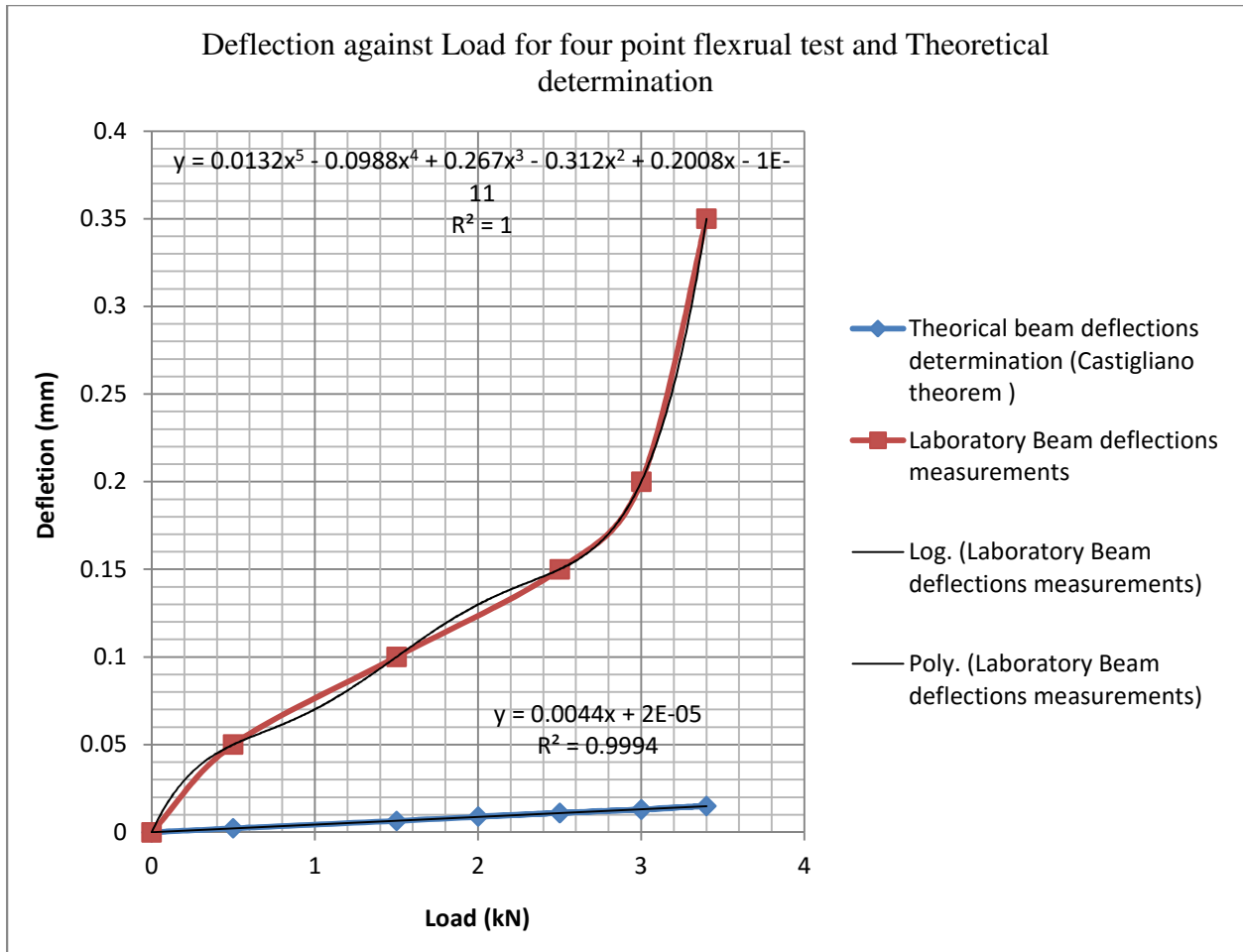| P (kN) | P(N) | Theoretical Deflection (mm) | Laboratory Deflections (mm) |
|---|---|---|---|
| 0 | 0 | 0 | 0 |
| 0.5 | 500 | 0.0022 | 0.05 |
| 1.5 | 1500 | 0.0065 | 0.1 |
| 2.5 | 2500 | 0.011 | 0.15 |
| 3 | 3000 | 0.013 | 0.2 |
| 3.4 | 3400 | 0.015 | 0.35 |
| 3 | 3000 | 0.013 | Beyond Elastic point |
| 2.5 | 2500 | 0.011 | |
| 2 | 2000 | 0.009 | |

Fig. 4.20: Comparison of theoretical and laboratory deflections.

### 4.9.3 Discussion

Laboratory and theoretical deflections model was developed, it was deduced that a factor i.e. $K_1$ related the two data sets.

$D_L = K_1 * D_T$; where $D_L$ denotes laboratory deflection, $D_T$ denotes theoretical deflection and $K_1$ is relationship factor dependent on the force.

$K_1$ was determined by dividing the polynomial equation developed from laboratory deflections and loads by the linear equation developed from theoretical deflections and loads. The resultant equation for $K_1$ was a quartic equation stated as:

$$K_1 = 3x^4 - 22.455x^3 + 60.68x^2 - 70.9x + 45.64$$
(Equation 4.9.1)

Where x is the force in kN.

The values for $K_1$ were therefore developed for a number of forces as shown below:

Table.4.18: Relationship factor $K_1$ for different loading.

| P (kN) | $K_1$ |
|--------|-------|
| 0 | - |
| 0.5 | 22.73 |
| 1.5 | 15.21 |
| 2.5 | 13.96 |
| 3 | 15.77 |
| 3.4 | 24.37 |

Ideally the factor would be a constant for all forces. The difference would be attributed by difference in data line of fit for both laboratory and experimental results due to either equipment calibrations or concrete quality and properties during testing.

## 4.10 Field measurements and Model Comparison

The model yielded a crack width of 0.137mm and a crack depth of 61.9mm, while the measured crack width and depth in the field ranged between 0.4-0.7mm and 86-149mm respectively. Laboratory deflections and theoretical deflections ranged between 0 to 0.35 and 0-0.015.

**4.10.1 Discussion**

Laboratory deflections compared with model crack width, there was a direct relationship between deflection value at failure and model crack width.

$$\Delta_F = CW \qquad\qquad \text{(Equation 4.10.1)}$$

In conclusion, the maximum deflection subjected to a beam to failure, i.e. cracking, influenced the amount of cracks formed, their sizes and the extent of opening.

# 5.0 CONCLUSION

a) Crack width and crack depth exhibited an exponential relationship in the S-math studio model; with the biggest crack having a maximum width of 0.2mm and a depth of 62mm. Experimentally they exhibited a degree five relationship with the biggest crack having a maximum width of 0.9mm and a depth of 130mm.Theoretically a linear relationship was noted.

S- math studio model was generated using predictive models based on vehicular loading; the difference is because there are other factors affecting the pavement and needed to be included in the models.

b) Both crack width and crack depth reduce with increased concrete rigidity. Rigidity has direct relationship with strength. Highly rigid pavements are more compact, and less susceptible to cracking.

From the mechanical modelling of the pavement shown in the figure below
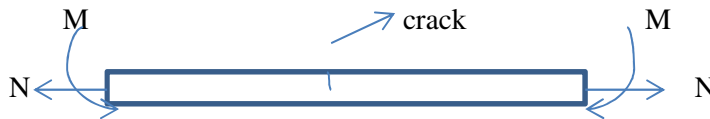


Rigidity (D) $= \dfrac{E * h^3}{12(1-v^2)}$

Where E is the Young Modulus of Concrete dependent on force applied in concrete (N/mm$^2$), h is the thickness of pavement (mm), and $v$ is the poison's ration of concrete

$E = \dfrac{F * l}{A * \Delta l}$ where F is the vehicular loading (N), l is the length of pavement slab (mm), A is the wheel load contact area (mm$^2$) and $\Delta l$ is the elongation (mm).

$$C_{mm} = \frac{2*l}{D}$$ where $C_{mm}$ is the compliance of pavement slab strip used to calculate slab

crack width   $C_{mm} = a/h$   where a is the crack width

Compliance is directly proportional to crack width and depth but inversely proportional

to rigidity.

c) Heavily loaded pavements would experience more tear and wear due to increased tensile

and compressive strength to the pavement.

Experimentally the safe load for Mbagathi road was determined as 430.4kN hence the

reason for cracks formation. The traffic load should be monitored against the safe load

presented in this report. This denotes a possibility of heavily loaded trucks with more

than 430.4 kN total truck load.

d) Transverse cracks

Major cracks developed are either longitudinal cracks which are parallel to the longer

dimension of the beam and transverse cracks which are perpendicular to the longitudinal

cracks. Transverse cracks were the most critical cracks since they were easily noticed, wide and

deep.

e) Cracks width and Beams deflection.

Cracks generated in a pavement due to the fatigue from repetitive loads beyond safe load.

Experimentally, there was a linear relationship developed between crack widths

determined from the model and deflections recorded during flexural testing of beams.

The amount of deflection induced by heavy vehicular loads in a concrete pavement beyond the elastic limit .i.e. at elastic-plastic point cracks induces cracks with a width approximately equivalent to the resultant deflection. Maximum flexural force of 3.4kN yielded a deflection of 3.5mm. Generally, a maximum deflection of 0.7mm was recorded after the beams were loaded beyond failure.

# 6.0 RECOMMENDATIONS

Based on this research, the following recommendations have been made:

1) Further research on concrete pavement should be done where additional causes of cracks should be considered since this study was limited to vehicular loading.

2) More predictive models on fracture mechanics should be studied and their results compared with results of this research. There were many predictive models available and all of them couldn't have been incorporated in this research.

3) The research was limited to a road pavement and in future there should be interest in other modes of transport like  air transport.

4) Deflections on both theoretical and laboratory methods were considered at elastic state. There is a need to extend deflections calculations to plastic state.

# REFERENCES

1. Dura, C., *Durability Design of Concrete Pavements*, Project BE95-1347/R14B, 2000.

2. Manual, M10, *Concrete Pavement Design and Construction*, Department of Transport, Pretoria, 1995.

3. Yang, H. H., *Pavement Analysis and Design Second edition*, Prentice Hall Pub , 2003

4. Zienkiewicz, O. C and Cheung, Y. K., *The Finite Element Method for Analysis of Elastic Isotropic and Orthotropic Slabs*, Institution of Civil Engineers- Proceedings, vol.28, pp.471-488, 1965.

5. Houben, Ir. L. J. M.., *Design of Concrete Pavements*, Part IV, 2009.

6. Kare, H., *Introduction to Fracture Mechanics*, McGraw-Hill Inc. US, 1984

7. Zdenek, P. B., *Fracture Mechanics of Concrete Structures*, Elsevier Applied Science, London and New York, 1992.

8. Zdenek, P. B., *Crack Band Theory for Fracture of Concrete*, Northwestern University, 1983.

9. Kare, H., *Introduction to Fracture Mechanics*, McGraw-Hill Inc. US, 1984.

10. Norbert J. D., *Concrete Pavement Design, Construction and Performance Second edition*, Taylor and Francis, 2008.

11. Guo H, J. A. Sherwood, and M.B. Synder*," Component Dowel Bar Model for Load Transfer Systems in PCC Pavements*," Journal of Transportation Engineering, , pp.287-297, May/June 1995.

12. Miner, M., *Cumulative Damage in Fatigue. American Society of Mechanical Engineers*, Journal of Applied Mechanics, 12 (3), 1945.

13. Alex, G., *A Mechanistic- Empirical Tie Bar Design Approach for Concrete Pavements*, Applied Research Associates, 2009.

14. BS 1881: Part 203, *Recommendations for Measurement of the Velocity of Ultrasonic Pulses in Concrete*, London, 1986.

15. Tada, H., P.C. Paris and G.R. Irwin*., The Stress Analysis of Cracks Handbook*. ASME Press, New York, 2008.

16. Bazant, Z.P., and Pfeiffer, P.A.,"*Determination of Fracture Energy Properties from Size Effect and Brittleness Number*," ACI Mater. J.,V.84, No.6, pp.468-480, 1987.

17. Farmington, H. M., , *Control of cracking in concrete,* American concrete institute, 1990.

18. Shah S.P., McGarry F.J., *Griffith Fracture Criterion and Concrete*, Journal of the Engineering Mechanics Division. ASCE Vol.97. No.EM6, Proc. Paper 8597, pp.1663-1676 , Dec. 1971.

19. Rice, J. R., *A Path Independent Integral and the Approximate Analysis of Strain Concentration by Notches and Cracks*. Transactions of ASME, Journal of applied mechanics, 35: 379-386, 1968.

20. Seong H. S., Paulino, G.H., and Buttlar, W.G, *Simulation of crack propagation in concrete using intrinsic cohesive zone model,* Transportation Research Board, Washington D.C, 2007.

21. Sansalone M. J., Lin J. W. B Street, *Determining the Depth of Surface Openings Cracks Using Impact Generated Stress Waves and Time of Flight Technique*," ACI Materials Journal. V.95.No.2., 1998.

22. Shin, S.W., Popovics, J. S., *Crack Depth Determination in Concrete Using Energy Transmission of Surface Waves*, ACI Materials. Vol.105.No.5, 2008.

23. Adoyo, F.O., *Pavement Evaluation of Mbagathi Road, Kenya.* Department of Civil Engineering. Nairobi University, 2012.

24. Chatti. K., Lysmer. J., Monismith. C,. *Dynamic Finite Element Analysis of Jointed Concrete Pavements,* Department of Civil Engineering. University of California, 1994.

25. Newton. P., Jackson. Nichols. Consulting,. *Development of revised pavement condition indices for Portland cement concrete pavement for the WSDOT pavement management system,* State Transportation Center. Washington, 2009.

26. F. Fuchs, A. Jasienski., *Manual for the execution of cement concrete pavements*, Belgian Road Research Centre, 1988.

27. Gerald F. Voigt., Early Cracking of Concrete Pavement- Causes and Repair, American Concrete Pavement Association, 2002.

28. Arne Hillerborg., *Application of Fracture Mechanics to Concrete*, Summary of a series of lecture notes, 1988.

29. Steven. M, 'Jointed Reinforced Concrete Pavement', 2009. [Online]. Availability: http://www.pavementinteractive.org/article/jointed-reinforced-concrete-pavement/ [Accessed: 14 – Feb – 2015].

# APPENDICES

Appendix-1: Crack depth determination Reference[1]

Appendix- 2: Laboratory testing photos

---

[1] ultrasound, surface opening cracks is a non-destructive testing

# Appendix-1: Crack depth determination Reference

## 2. Methods to estimate crack depth

### 2.1 Existing Methods

Bungey [3] proposed a mathematical expression by comparing the time-of-flight of an ultrasound longitudinal wave through a sound concrete to the one around a crack, considering that the velocity of the longitudinal wave in the concrete is the same in both cases. Assuming the wave travel path presented in Fig. 1a, the crack penetration depth "h" can be evaluated as:

$$h = \left(\frac{x}{T_s}\right)\sqrt{T_c^2 - T_s^2} \quad \dots\dots\dots\dots\dots\dots\dots\dots \text{(1)}$$

where: $T_c$ represents the travel time around the crack; $T_s$ is the surface travel time in sound concrete, and $x$ is the least distance between the transducers and the crack, measured on the surface of the concrete. In order to use Eq. 1, it is necessary to previously obtain the surface travel time of the longitudinal wave in a region without crack, $T_s$, with transducers at a distance $2x$ apart from each other.

The assumption of the same ultrasonic pulse velocity through a sound surface concrete and through a path around the crack may lead to errors in the estimate of the crack depth. Usually, top concrete layers are more porous than inner parts due to differences in settlement

of aggregates, vibration and also humidity loss to the environment. Thus, it is common to observe a smaller UPV in the surface of the concrete than in the inner parts of the structure. Bungey [3] states that the depth of surface opening cracks using Eq. 1 can be estimated with a precision of 15%.

Another method to estimate the depth of surface opening cracks is the one presented in BS 1881: Part 203 [2]. This method uses two measurements taken with the transducers placed equidistantly from the crack at the distances $x$, and $2x$, according to Fig. 1b. Assuming that the ultrasonic pulse velocity is the same, it is possible to modify Eq. 1, as follows:

$$h = x \sqrt{\frac{4T_1^2 - T_2^2}{T_2^2 - T_1^2}} \quad \dots\dots\dots\dots\dots\dots\dots\dots \text{(2)}$$

where $T_1$ and $T_2$ are the time-of-flight of the longitudinal wave with transducers at distances $x$, and $2x$ from the crack, respectively. BS 1881 [2] suggests a distance $x$ of 15 cm.
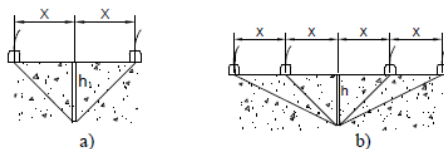


Fig.1. Transducer arrangements for Bungey's and BS 1881 methods

Appendix- 2: Laboratory testing photos



Photo A2-1: Cubes tested with the crushing strength machine



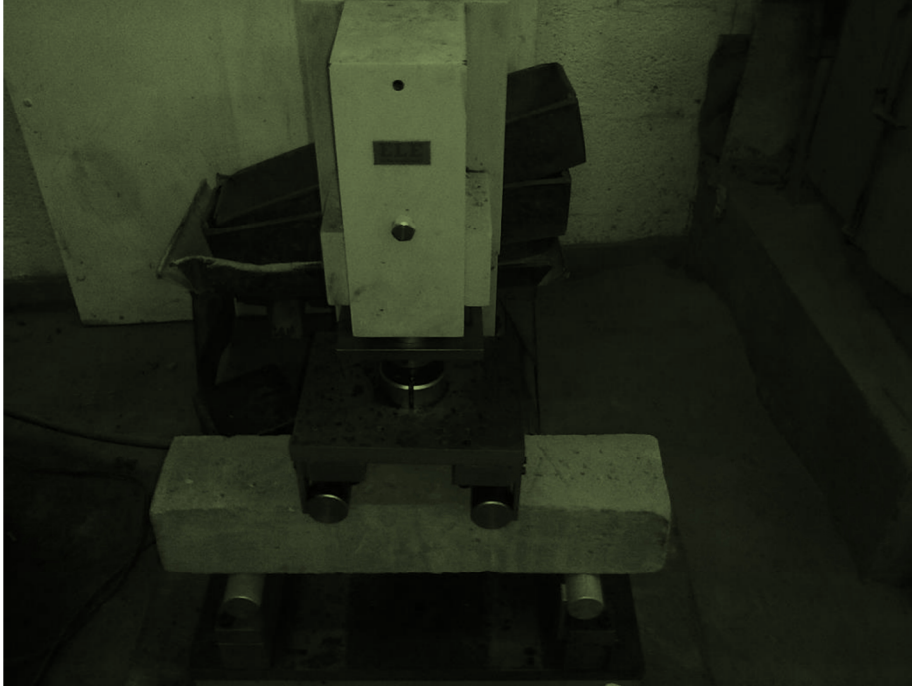Photo A2-2: Beams cast for flexural testing
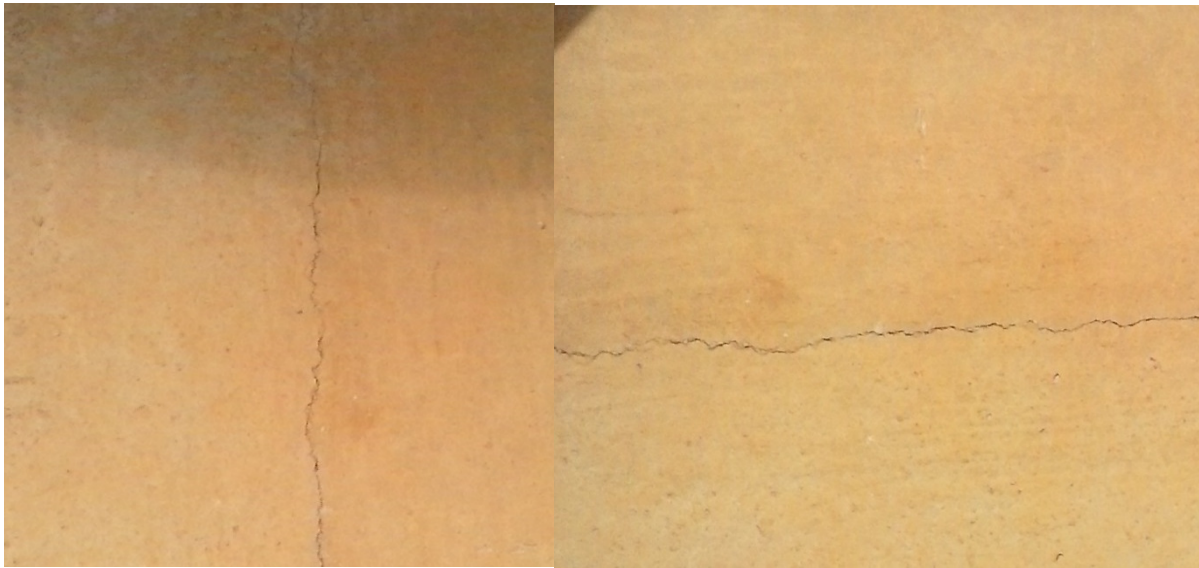
Photo A2-3: A beam being set on flexural testing



Photo A2-4: Observed failure during flexural test in beams.